

The High Mass Slope of the IMF

Antonio Parravano^{1,2*}, David Hollenbach³ Christopher F. McKee⁴

¹Universidad de Los Andes, Centro De Física Fundamental, Mérida 5101a, Venezuela

²Universidad de Málaga, Málaga, Spain

³SETI Institute, 189 Bernardo Avenue, Mountain View, CA 94043

⁴Physics Department and Astronomy Department, University of California at Berkeley, Berkeley, CA 94720

Accepted XXX. Received YYY; in original form ZZZ

ABSTRACT

Recent papers have found that the inferred slope of the high-mass ($> 1.5 M_{\odot}$) IMF for field stars in the solar vicinity has a larger value ($\sim 1.7 - 2.1$) than the slopes ($\sim 1.2 - 1.7$; Salpeter = 1.35) inferred from numerous studies of young clusters. We attempt to reconcile this apparent contradiction. Stars mostly form in Giant Molecular Clouds, and the more massive stars ($\gtrsim 3 M_{\odot}$) may have insufficient time before their deaths to uniformly populate the solar circle of the Galaxy. We examine the effect of small sample volumes on the *apparent* slope, Γ_{app} , of the high-mass IMF by modeling the present day mass function (PDMF) over the mass range $1.5 - 6 M_{\odot}$. Depending on the location of the observer along the solar circle and the size of the sample volume, the apparent slope of the IMF can show a wide variance, with typical values steeper than the underlying universal value Γ . We show, for example, that the PDMFs observed in a small (radius ~ 200 pc) volume randomly placed at the solar circle have a $\sim 15 - 30\%$ likelihood of resulting in $\Gamma_{\text{app}} \gtrsim \Gamma + 0.35$ because of inhomogeneities in the surface densities of more massive stars. If we add the a priori knowledge that the Sun currently lies in an interarm region, where the star formation rate is lower than the average at the solar circle, we find an even higher likelihood ($\sim 50 - 60\%$) of $\Gamma_{\text{app}} \gtrsim \Gamma + 0.35$, corresponding to $\Gamma_{\text{app}} \gtrsim 1.7$ when the underlying $\Gamma = 1.35$.

Key words: stars: formation – stars: luminosity function, mass function – galaxies: star clusters: general – galaxies: spiral – Galaxy: solar neighbourhood

1 INTRODUCTION

The stellar initial mass function (IMF) is of fundamental importance in astrophysics because it relates the relative number of high-mass stars that produce most of the light and energy to the low-mass stars that make up most of the stellar mass. In distant and/or dust-obscured regions of the Galaxy and in external galaxies, it is often the case that only the high-mass stellar component can be measured, whether through direct emission from the massive stars, from emission from the HII regions surrounding these stars, or through reprocessed infrared radiation. If the IMF is known, such observations can be used to estimate the total star formation rate (SFR). More generally, as Weisz et al. (2015) have pointed out, knowing the IMF of stars “is essential to interpreting the stellar populations of star-forming galaxies across cosmic time, testing and validating theories of star formation, constraining models of chemical evolution, the formation of compact objects, and understanding the interplay between stars and gas.”

There is considerable evidence that the IMF in disk galaxies is universal (Renzini 2005, Bastian et al. 2010, Offner et al. 2014); in particular, the last authors conclude that studies of resolved stellar populations provide no evidence for variations of the IMF within local galaxies that are greater than 2σ . For stellar masses $m \gtrsim 1$ (in this paper, all stellar masses are in units of the solar mass), the IMF has been usually modeled as a power law, $\psi(m) \propto m^{-\Gamma}$ up to a limiting mass ~ 100 , where Γ is the underlying universal slope of the high-mass IMF (Bastian et al. 2010). These reviews conclude that the observations are consistent with $\Gamma \simeq 1.35$, the Salpeter value. The value of this power law is particularly important, since it regulates the relative number of low- and high- mass stars. One reason the underlying IMF may be universal is that current theories of the origin of the IMF are based on turbulence, so the slope is independent of the density, chemistry and other properties. It depends primarily on the exponent p in the linewidth-size relation $\sigma \propto r^p$ (e.g., Hopkins 2012; for supersonic turbulence, $p \simeq 0.5$ (e.g., Hennebelle & Falgarone 2012).

On the other hand, there is observational evidence for deviations from a universal IMF in extreme environments:

* E-mail: parravan3@gmail.com

Lu et al. (2013) find a smaller value of Γ in the Galactic Center clusters, as do Schneider et al. (2018) in 30 Dor. A number of workers have found evidence for a bottom heavy IMF in giant ellipticals (e.g., van Dokkum & Conroy 2010, Cappellari et al. 2012). We note that it has been suggested that the IMF on galactic scales is the superposition of cluster IMFs that obey a relation between the maximum stellar mass and the mass of the cluster (e.g., Kroupa & Weidner 2003, Kroupa et al. 2013 and references therein). Evidence against this hypothesis and in favor of the hypothesis that cluster IMFs are the result of random sampling from a universal IMF is summarized in Ashworth et al. (2017). In this paper we adopt the latter hypothesis, at least in the Milky Way outside its nucleus, and we examine reasons why the observed ratio of high mass to low mass stars might vary from region to region.

1.1 IMF from Clusters and IMF from Local Field Stars

Observations of stellar clusters (including stellar associations) that are young enough that none of the stars within a specified mass range have evolved off the main sequence allow a direct estimate of Γ , and we define the slope inferred from such observations as Γ_c . The primary advantage of using cluster studies over field-star studies to infer the slope of the IMF is that the stars in clusters were all born at approximately the same time and have the same distance and metallicity. Even with this simplification, however, a number of problems remain with inferring the high-mass slope from cluster studies (Scalo 2005): (i) Most clusters studied have a small number of stars per mass bin or a very small number of bins; (ii) the ubiquity of mass segregation means that clusters must be observed to large radii; (iii) membership is a problem, especially at large radii; (iv) the correction for unresolved binaries is uncertain; (v) adopted cluster properties (distance, age, metallicity, extinction, and differential reddening) can introduce errors; and (vi) uncertainties in evolutionary tracks and isochrones affect mass determinations. Therefore it is difficult to determine if the large variation in the inferred values of Γ_c from cluster to cluster is due to variations in the IMF or to the uncertainties introduced by these problems.

Weisz et al. (2015) reviewed the cluster literature on the high-mass slope and concluded that most of the studies found $1.2 \lesssim \Gamma_c \lesssim 1.7$. By studying a large number (85) of clusters in M31, they were able to eliminate almost all the problems listed above. They concluded that the intrinsic high-mass ($m > 2$) slope there is $\Gamma_c = 1.45^{+0.03}_{-0.06}$ and that this high-mass slope for the 85 clusters is universal.

To determine the IMF from observations of field stars, observers/modelers match synthetic populations to counts of stars in the color-magnitude diagram. These population synthesis simulations assume evolutionary tracks, stellar atmosphere models, a given time evolution of the SFR (the star formation history, or SFH), vertical diffusion, binary frequency as a function of mass, and a model for interstellar extinction. The simulations are run with various underlying values of Γ , and the best fit to the observations provides the apparent slope of the field star IMF, $\Gamma_{f,\text{app}}$. Here the subscript ‘‘app’’ indicates that this is the apparent value one would obtain after attempting to allow for all the uncertain-

ties just enumerated, but assuming that stars are distributed uniformly in the plane of the Galaxy. In fact, however, stars are not uniformly distributed in the plane because star formation is highly inhomogeneous in both space and time, and the focus of this paper is on the effects that this non-uniform distribution of stars, particularly the more massive and therefore younger ones, have on the inferred high-mass slope of the IMF.

1.2 Three Recent Determinations of the High-Mass Slope of the IMF from the Local Field

In contrast to the determinations of $\Gamma_c \simeq 1.2 - 1.7$ in the Milky Way and other galaxies, there have been three recent determinations of the apparent slope of the field-star IMF in the solar neighborhood that have yielded higher values, $\Gamma_{f,\text{app}} \simeq 1.7 - 2.1$ (Dawson & Schröder 2010, Czekaj et al. 2014, and Rybizki & Just 2015). These papers assume a smooth distribution of the SFR in the plane of the Galaxy and attempt to account for binarity, the SFH and the age-dependent vertical distribution of stars; the radial gradient of the SFR is neglected in these studies due to the small size of the observational volumes.

Dawson & Schröder (2010) used Hipparchos data to create a sample of stars with $m > 0.9$, within a radius of 100 pc of the Sun, and within ± 25 pc of the Galactic plane. They compared synthetic simulations that included the effect of unresolved binaries and the effect of age-dependent vertical diffusion of stars. For their favored binary model, in which the binary fraction (including multiples) is 71%, they found $\Gamma_{f,\text{app}} \simeq 1.85 \pm 0.15$. If they allowed the binary fraction to decrease with mass from 71% for primary stars just above $3M_\odot$ to 57% for primary stars just above $1M_\odot$, they found $\Gamma_{f,\text{app}} \simeq 2.2$, but this binary model was not favored by their data. They concluded that the SFR has been ‘‘reasonably’’ constant during the lifetime of the stars in their sample, but they did not quantify how much it could have changed over the last 3 Gyr, the time period which we focus on in this paper (roughly the lifetime of a $m = 1.5$ star). One problem with inferring SFH was the uncertainty in the rate of vertical diffusion of stars out of their observing volume as a function of stellar age.

Czekaj et al (2014) compared synthetic distributions of the number of stars plotted against B-V with Hipparchos (Tycho-2) data and estimated that $\Gamma_{f,\text{app}} \sim 2$ in the solar neighborhood. In contrast to Dawson & Schröder (2010) and Rybizki & Just (2015), they considered stars over a wide mass range, although the main fitting of the model to data was to Tycho-2 data, which is a magnitude limited sample down to $V = 11$. They used an updated version of the Besancon Galaxy model and tested several different SFHs, IMFs, evolutionary tracks, and dust extinction models against the data. They corrected for the effect of binaries by using the binary fraction determined by Arenou (2011), which varies from about 0.1 for $m = 0.1$ to 0.84 at very high masses. The SFHs include both a constant SFR and a rate that declines as $\exp(-t/t_{\text{SFR}})$, where $t_{\text{SFR}} = 8.3$

Gyr (Aumer & Binney 2009).¹ They focused on stars with $V < 11$, which means that the volume included around the Sun depends on the stellar luminosity as well as the dust extinction corrections; stars of mass $m \sim 1.5$ are included in their sample provided they are within about 300 pc for a typical amount of extinction. There is no error estimate possible in this study because it included only 5 different values of Γ in the simulations: two simulations with $\Gamma = 1.3$, six with $\Gamma = 2.0$, one with $\Gamma = 2.2$, one with $\Gamma = 2.5$, and one with $\Gamma = 3.16$. The chi squared fits favor $\Gamma = 2$ for these simulations; the $\Gamma = 1.3$ and $\Gamma = 3.16$ cases have values of chi squared that are about 3 times larger than the favored case. However, there are no simulations with Γ between 1.3 and 2, so we cannot know where the minimum chi squared occurs. The authors concluded that $\Gamma_{f,\text{app}}$ is larger than 1.3 and is about 2.

Analyzing stars within 200 pc from Hipparcos and from the Catalogue of Nearby Stars, Rybizki & Just (2015) improved upon an earlier paper by Just & Jahreiß (2010) and found that a better treatment of binarity and reddening reduced $\Gamma_{f,\text{app}}$ from 3.16 in Just & Jahreiß (2010) to 2.02 ± 0.06 for the mass range $1.4 < m < 10$. This demonstrates the sensitivity of the inferred value of $\Gamma_{f,\text{app}}$ to these corrections. Their adopted SFH scales as $\exp(-t/t_{\text{SFR}})$ (Aumer & Binney 2009) for the last several Gyr (again with $t_{\text{SFR}} = 8.3$ Gyr). They also allowed for vertical diffusion of stars with age. The quoted errors are very small, but as the authors note, these errors do not include systematic errors due to uncertainties in the binary correction, the inhomogeneous ISM, variable stars, the thick disk component, the metal enrichment law, and low mass stellar envelopes.

Given the discussion above, we take these three papers in aggregate to indicate that the apparent value of the high-mass slope of the IMF, after correction for a possible decline in the SFR with time and for vertical diffusion of stars due to disk heating, is $\Gamma_{f,\text{app}} \simeq 1.7 - 2.1$ in the solar neighborhood. We note the sample volumes in Dawson & Schröder (2010) and Rybizki & Just (2015) are relatively small, with radii < 200 pc.

1.3 Summary of Goals of the Paper and the Methodology of our Simulations

In this paper we explore the possibility that the apparent discrepancy between the estimates from young clusters and galaxies discussed in the above reviews, which have $\Gamma_c \sim 1.2 - 1.7$, and the local estimates of $\Gamma_{f,\text{app}} \simeq 1.7 - 2.1$ can be explained by clustered star formation and by the location of the Sun in an interarm region. Our simulations isolate the effect of the inhomogeneous distribution of higher mass ($m \gtrsim 3$) stars on the inference of the high-mass IMF slope when observing finite volumes at the solar circle.

Massive stars have an inhomogeneous distribution in the Galactic plane because they are mostly born in massive GMCs that sparsely populate the Galaxy, and their short lifetimes do not allow them to move from these localized birthsites to uniformly populate the plane. Lower mass stars live longer, so they diffuse from their birth sites and spread

more uniformly in the plane. Thus, there will be substantial volumes of Galactic space around the solar circle with a relative deficit of higher mass stars (high $\Gamma_{f,\text{app}}$), and at the same time smaller volumes that include significant sites of recent star formation with relatively high numbers of higher mass stars (low $\Gamma_{f,\text{app}}$). Furthermore, the Sun is not randomly placed along the solar circle, but in an interarm region, where the SFR has been depressed compared to the solar circle average for ~ 100 Myr. As Elmegreen & Scalo (2006) have pointed out, this has most likely steepened the PDMF and could lead to the erroneous inference that the high-mass slope of the IMF is steeper than it actually is.

The simulations we present in this paper can be summarized as follows (details in Section 3). Our simulation volume includes a large portion of the solar circle. Stars are born with an IMF characterized by an underlying Γ inside widely separated GMCs, and they then move from their birthsites to fill the volume of the simulation. Their velocities are prescribed from observations of stellar velocity dispersions in the plane of the Galaxy. Given these velocities, there is not enough time during their lifetimes for the higher mass stars to homogenize; the higher the mass, the shorter the lifetime and therefore the greater the fluctuation in density. We follow stars of mass $m = 1.5 - 6$ because $m \gtrsim 1.5$ ensures we are on the high mass slope part of the IMF, and because a range of mass is needed to provide an accurate measure of slope.² In order to make our procedure more closely parallel what the observers do, we include the effects of a time dependent SFR and an age-dependent vertical diffusion in our simulation and then remove these effects afterwards in the same manner that observers would. We run the simulation for 3 Gyr so that we get a full sample of all MS stars with mass $m > 1.5$. At the end of the simulation we know the location and mass of each of the roughly 2×10^7 stars in the simulation. We measure the PDMFs in random small (radius $\sim 100 - 750$ pc) volumes at the solar circle in each simulation. The PDMFs vary from volume to volume, and from their distribution we infer a distribution function of the apparent $\Gamma_{f,\text{app}}$ given a fixed universal value of Γ for stellar birth.

In contrast to the value of $\Gamma_{f,\text{app}}$ from observations, which can differ from the underlying value of Γ due to the clustering of star formation in space and time as well as to many other errors introduced by the comparison of observations with the population synthesis simulations, the apparent value of Γ inferred from the simulations, Γ_{app} , differs from Γ only because of the clustering. For the relatively small volumes in the papers cited above, the PDMFs of the $m \gtrsim 1.5$ stars can differ significantly from that due to a uniform distribution of stars, resulting in a significant probability of finding $\Gamma_{\text{app}} > \Gamma$ from a randomly chosen observational location at the solar circle. The effect is larger if one considers that the Sun is not in a random position but in an interarm position.

The purpose of our simulations is not to compare simulation with observation directly, but rather to demonstrate

¹ Note that this is equivalent to the form $\exp(-0.12t_{\text{Gyr}})$, where t_{Gyr} is $t/1$ Gyr. This form is often seen in the literature.

² Because of the steepness of the PDMF, our measure of the slope depends mostly on the ratio of $m = 3$ stars to $m = 1.5$ stars, so that the results do not depend sensitively on the upper limit value $m = 6$ (as will be discussed further in Section 2).

the effect that the inhomogeneous distribution of stars can have in estimating Γ . Our simulations provide a quantitative estimate of the magnitude of this single effect.

Section 2 presents the basic theory that relates the IMF to the PDMF, and a simple analytic fit to the stellar lifetimes that enables an analytic solution to the PDMF. Section 3 presents our model for the spatial distribution of stars of various masses at the solar circle, given that stars are born in GMCs and diffuse from these formation sites. These numerical simulations are repeated numerous times, and from these simulations we determine the distribution of Γ_{app} as a function of the volume of space sampled in observationally determining the PDMF. Section 4 focusses on the effect of spiral arms, providing representative examples of the effects that spiral arms could have on the distribution of Γ_{app} . Finally, in Section 5 we present a summary and our conclusions, and note the relevance of these results to the Gaia data.

2 INFERRING THE HIGH-MASS IMF FROM THE PDMF

In this section we derive analytical expressions that relate the PDMF to the IMF. Although the high-mass portion of the IMF is well characterized by a power law (Bastian et al. 2010), the high-mass PDMF is not necessarily so described. We therefore consider a range of masses, $m=1.5$ to 6, chosen to be well represented in the observational studies of Dawson & Schröder (2010), Czekaj et al. (2014) and Rybizki & Just (2015) and to lie clearly in the high mass regime of the IMF. We characterize the PDMF here and in our simulations by the ratio \mathcal{R} of lower mass ($1.5 < m < 3$) stars to higher mass ($3 < m < 6$) stars in a given finite volume:

$$\mathcal{R} \equiv \frac{\mathcal{N}_*(1.5 < m < 3)}{\mathcal{N}_*(3 < m < 6)}. \quad (1)$$

Due to the steepness of the PDMF, this ratio is essentially the ratio of stars with mass $m \sim 1.5$ to stars with mass $m \sim 3$. Under the assumption of a homogeneous distribution of stars of all masses in the plane of the Galaxy, we analytically derive below how the relation of \mathcal{R} to the underlying Γ varies due to the SFH (constant SFR versus declining SFR) and age-dependent vertical diffusion. The latter effect depends on the volume sampled and we show this dependence. In Section 3 we treat the effect of the inhomogeneous distribution of stars of various masses in the plane of the Galaxy due to their localized (in time and space) births. This effect is not amenable to an analytic treatment and so is not included in this section.

We emphasize that we use the ratio \mathcal{R} to characterize the PDMF and to infer the IMF in our simulations. The papers that compare population synthesis models with observations do not use this ratio. However, in essence, they are comparing the densities of higher mass and lower mass stars in a given volume to infer the slope of the IMF, so their method is analogous to ours. The point of the simulations is not to completely mimic the population synthesis methods, but to isolate the effect that the localized star formation has on the inference of the IMFs from observed PDMFs in small volumes. An advantage the simulations is that we know the

masses of the stars and their locations, so there are no errors caused by model atmospheres, distance ambiguities, binary corrections, observational errors, etc.

2.1 The IMF and the PDMF

We begin by relating the high-mass portion of the IMF to the total IMF. Let $\psi(m)d\ln m$ be the fraction of stellar objects (including brown dwarfs) born in the mass range m to $m+dm$. In Parravano, McKee & Hollenbach (2011, henceforth Paper I), we adopted the functional form for the IMF,

$$\psi(m) = Cm^{-\Gamma} \{1 - \exp[-(m/m_{\text{ch}})^{\gamma+\Gamma}]\}, \quad (2)$$

where C is a normalization constant such that

$$\int_{m_{\text{el}}}^{m_{\text{u}}} \psi(m)d\ln m = 1. \quad (3)$$

This form for the IMF approaches a power law both at low stellar masses,

$$\psi \rightarrow Cm_{\text{ch}}^{-\Gamma} \left(\frac{m}{m_{\text{ch}}}\right)^{\gamma}, \quad (4)$$

and at high stellar masses,

$$\psi \rightarrow Cm^{-\Gamma}, \quad (5)$$

and we termed it the Smoothed Two-Power Law (STPL) form for the IMF. Assuming $\Gamma = 1.35$, we determined best fit values of $\gamma = 0.51$ and $m_{\text{ch}} = 0.35$, corresponding to $C = 0.108$, for the solar neighborhood. Insofar as the IMF is universal, as discussed in Section 1, this IMF should be generally valid in disk galaxies.

We note that other authors have adopted different functional forms for the IMF, but there is general agreement that for $m \gtrsim 1$, the IMF follows a power law $\psi(m) \propto m^{-\Gamma}$ (Bastian et al. 2010). Because this paper treats stars with $m > 1.5$, we adopt here the high-mass form from Equation (5), $\psi(m) = Cm^{-\Gamma}$ (this form agrees with Equation 2 to better than 0.1% for $m > 1$).

The differential star-formation rate by number as a function of mass and time is given by $d\dot{\mathcal{N}}_*(m,t)/d\ln m$, where $\dot{\mathcal{N}}_*(m,t)$ includes only stellar births, not stellar deaths and where m is the initial mass of the star. This rate can be expressed as the product of the total star-formation rate by number, $\dot{\mathcal{N}}_{*T}(t)$, and the probability that a star is born with a mass m —i.e., the IMF, $\psi(m)$:

$$\frac{d\dot{\mathcal{N}}_*(m,t)}{d\ln m} = \dot{\mathcal{N}}_{*T}(t)\psi(m). \quad (6)$$

The PDMF can be expressed as $d\mathcal{N}_*(m)/d\ln m$, where $d\mathcal{N}_*(m)$ is the number of stars with masses between m and $m+dm$ at the present epoch, $t = t_0$. This form of the PDMF is about equal to the number of stars in a mass interval of a factor e around m . To relate the PDMF to the IMF, we make two assumptions: First, we assume that the stellar mass is about constant in time as the star ages—i.e., we focus on main sequence stars that are not too massive. Second, we assume that the volume in which the PDMF is measured includes all the surviving main sequence stars that were formed. Then the PDMF is the time integral of the star formation rate,

$$\frac{d\mathcal{N}_*(m)}{d\ln m} = \int_{t_0-\tau'(m)}^{t_0} \dot{\mathcal{N}}_{*T}(t)\psi(m) dt, \quad (7)$$

where $\tau' \equiv \min[\tau_{\text{MS}}(m), t_0]$ and $\tau_{\text{MS}}(m)$ is the main sequence lifetime of a star of mass m (e.g., [Scalo 1986](#)). For the particular case of stars with $m \gtrsim 1$, so that $\tau_{\text{MS}}(m) < t_0$, and for a constant star formation rate, the PDMF is simply

$$\frac{d\mathcal{N}_*(m)}{d\ln m} = \mathcal{N}_{*T} \psi(m) \tau_{\text{MS}}(m). \quad (8)$$

We note a similar derivation in the [Prantzos \(2008\)](#) review (Eqs. 2.20, 2.2.1).

2.2 Relation of \mathcal{R} to IMF Slope for Constant SFR

The main effect that alters the value of \mathcal{R} (see Eq. 1) from its initial value is stellar evolution, since the more massive the star, the more rapidly it evolves off the main sequence. If the SFR has been constant for more than the lifetime of a $m = 1.5$ star, \mathcal{R} can be derived from Equation 8:

$$\mathcal{R}_0 = \frac{\int_{1.5}^3 \tau_{\text{MS}}(m) \psi(m) d\ln m}{\int_3^6 \tau_{\text{MS}}(m) \psi(m) d\ln m}, \quad (9)$$

where the subscript “0” refers to the assumptions of constant SFR, no vertical segregation by mass, and homogeneous distribution in the plane of the Galaxy. Using main sequence lifetimes from [Bressan et al. \(2012\)](#) (for example the lifetimes of stars of mass $m = 1.5, 3$, and 6 with solar metallicity are 2570 Myr, 354 Myr and 69 Myr, respectively), we have numerically integrated Equation (9) and found that $\mathcal{R}_0 = 16.9$ for $\Gamma = 1.35$. On the other hand, $\mathcal{R}_0 = 26.6$ for $\Gamma = 2$, substantially higher. This gives an idea of how many $m = 3 - 6$ stars would need to be depleted in order for our inferred Γ_{app} to be 2 and not 1.35 : One needs to lower $\mathcal{N}_*(3 < m < 6)$ by $[1 - (16.9/26.6)] \times 100 = 36\%$.

We can obtain an approximate expression for \mathcal{R}_0 by approximating the main sequence lifetimes of stars in the range $1.5 < m < 6$,

$$\tau_{\text{MS}}(m) \simeq 390 \left(\frac{m}{3}\right)^{-2.72} \text{ Myr}, \quad (10)$$

which fits the lifetimes to within 9%. With this power law, $\tau_{\text{MS}}(m) \psi(m)$ is proportional to $m^{-2.72-\Gamma}$, and we can analytically compute the ratio \mathcal{R}_0 for arbitrary Γ :

$$\mathcal{R}_0 \simeq 2^{2.72+\Gamma}. \quad (11)$$

The values of \mathcal{R}_0 obtained with this power law are accurate to within 1% for $1 < \Gamma < 2$. For example, assuming $\Gamma = 1.35$ ($\Gamma = 2.0$), this approximation gives $\mathcal{R}_0 = 16.8$ ($\mathcal{R}_0 = 26.4$) in excellent agreement with the exact values.

This equation can be rearranged to provide an approximation for the inferred $\Gamma_{\text{app},0}$ if the ratio \mathcal{R} is observed in some volume of the Galaxy or of our simulation:

$$\Gamma_{\text{app},0} \simeq 1.44 \ln \mathcal{R} - 2.72. \quad (12)$$

This would provide a good estimate of Γ , the underlying slope of the universal IMF, only if there were no vertical stellar diffusion, no time dependence of the SFR over the last 2.6 Gyr, and no spatial variation in the SFR. Discussion of these effects, especially the last effect, occupies much of the rest of this paper.

2.3 Approximation for a Declining SFR

We treat the simple case of the SFR rate declining as $\mathcal{N}_{*T}(t) \propto \exp(-t/t_{\text{SFR}})$, with $t_{\text{SFR}} = 8.3$ Gyr for numerical

evaluation ([Aumer & Binney 2009](#)). Define $t' \equiv t_0 - t$. Equation (6) then gives

$$\begin{aligned} \frac{d\mathcal{N}_*(m)}{d\ln m} &= \mathcal{N}_{*T}(t_0) \psi(m) \int_0^{\tau_{\text{MS}}(m)} e^{t'/t_{\text{SFR}}} dt', \quad (13) \\ &= \mathcal{N}_{*T}(t_0) \psi(m) t_{\text{SFR}} \left[e^{\tau_{\text{MS}}(m)/t_{\text{SFR}}} - 1 \right]. \quad (14) \end{aligned}$$

Since we are now including only the first effect that can alter the observed value of \mathcal{R} , a time-varying star formation rate, we label the resulting value of \mathcal{R} as \mathcal{R}_1 . To solve analytically for the ratio \mathcal{R}_1 requires that we expand the exponential as a power series in the quantity $\tau_{\text{MS}}(m)/t_{\text{SFR}}$, which is small for $m = 1.5 - 6$ stars and our adopted decay time. This then gives the solution

$$\frac{d\mathcal{N}_*(m)}{d\ln m} \simeq \mathcal{N}_{*T}(t_0) \psi(m) \tau_{\text{MS}}(m) \left[1 + \frac{\tau_{\text{MS}}(m)}{2t_{\text{SFR}}} \right]. \quad (15)$$

Evaluating \mathcal{R} from Equation (1), we find

$$\mathcal{R}_1 \simeq 2^{2.72+\Gamma} \left(\frac{1+B}{1+2^{-2.72}B} \right), \quad (16)$$

where the subscript “1” refers to the assumption of an exponentially declining SFR, as well as no vertical segregation by mass and homogeneous distribution in the plane of the Galaxy, and where

$$B \equiv \frac{1}{2 \times 1.5^{2.72}} \left(\frac{2.72+\Gamma}{5.44+\Gamma} \right) \left(\frac{1-2^{-(5.44+\Gamma)}}{1-2^{-(2.72+\Gamma)}} \right) \left(\frac{7.74 \text{ Gyr}}{t_{\text{SFR}}} \right). \quad (17)$$

Since $B \sim 0.1$ is small, \mathcal{R}_1 can be approximated as

$$\mathcal{R}_1 \simeq 2^{2.72+\Gamma+(1.2 \text{ Gyr})/t_{\text{SFR}}}, \quad (18)$$

which is accurate to within 2.4% for $1 < \Gamma < 2$. Correspondingly, if the ratio of $m = 1.5 - 3$ stars to $m = 3 - 6$ stars is \mathcal{R} , then the value of Γ inferred under the assumption that the only effect altering \mathcal{R} is an exponentially declining SFR is

$$\Gamma_{\text{app},1} \simeq 1.44 \ln \mathcal{R} - 2.72 - (1.20 \text{ Gyr})/t_{\text{SFR}}. \quad (19)$$

We recover $\Gamma_{\text{app},0}$ for a constant SFR ($t_{\text{SFR}} = \infty$). Because the notation becomes somewhat complicated, we present in Table 1 a list of parameters and their definitions.

For $t_{\text{SFR}} = 8.3$ Gyr and $\Gamma = 1.35$, we have $\mathcal{R}_1 \simeq 18.6$. Had we assumed a constant SFR (as [Dawson & Schröder 2010](#) did) and had we used this ratio to determine Γ_{app} from Equation (12), then we would have obtained $\Gamma_{\text{app}} = 1.49$ instead of the underlying $\Gamma = 1.35$. Hence, a declining SFR with $t_{\text{SFR}} = 8.3$ Gyr can account for only a part of the discrepancy between the underlying Γ and the value $\Gamma_{\text{app}} \simeq 1.85$ derived from limited volumes around the Sun by [Dawson & Schröder \(2010\)](#). We can use Eqs (11) and (18) to derive that $t_{\text{SFR}} = 2.4$ Gyr is needed to produce $\Gamma_{\text{app},0} = 1.85$ if the underlying $\Gamma = 1.35$ and the star formation is declining as given by t_{SFR} . Such a rapidly decreasing SFR has not been inferred in studies of the SFH over the past ~ 3 Gyr. Similarly, although the studies of [Czekaj et al. \(2014\)](#) and [Rybizki & Just \(2015\)](#) assumed $t_{\text{SFR}} = 8.3$ Gyr, the true t_{SFR} would have to be much smaller in order for their results $\Gamma_{f,\text{app}} \sim 2$ to be consistent with an underlying $\Gamma \sim 1.2 - 1.7$. Such a small t_{SFR} seems unlikely. Instead, the explanation for why the recent field star results find $\Gamma_{f,\text{app}} \sim 1.7 - 2.1$ compared to what could be a much lower underlying Γ may

Table 1. Definitions

\mathcal{R}	Ratio of $m = 1.5 - 3$ stars to $m = 3 - 6$ stars.
\mathcal{R}_0	Theoretical value of \mathcal{R} for a steady and uniform SFR.
\mathcal{R}_1	Theoretical value of \mathcal{R} for a declining SFR.
\mathcal{R}_{12}	Theoretical value of \mathcal{R} taking into account the effect of a declining SFR and the age-dependent vertical diffusion.
Γ	Slope (negative) of the individual IMF for over-solar stars.
$\Gamma_{\text{app},0}$	Value of Γ_{app} derived from \mathcal{R} when SFR is constant and uniform.
$\Gamma_{\text{app},1}$	Value of Γ_{app} derived from \mathcal{R} assuming a declining SFR.
$\Gamma_{\text{app},12}$	Value of Γ_{app} derived from \mathcal{R} taking into account the effect of a declining SFR and age-dependent vertical diffusion.
Γ_c	Value of Γ inferred from cluster observations.
$\Gamma_{f,\text{app}}$	Apparent value of Γ inferred from the PDMF of field-star in limited volumes.
Γ_{app}	Apparent value of Γ from simulations, generally after accounting for stellar evolution, a declining SFR, and vertical diffusion so that $\Gamma_{\text{app}} \equiv \Gamma_{\text{app},12}$.
$\Delta\Gamma_{\text{app}}$	Difference between Γ_{app} and the underlying Γ .

lie in the effect of clustered star formation, which we treat below in Section 3. However, first we treat the effect of the age dependent, and therefore mass dependent, vertical distribution of stars, which can affect the derivation of Γ from limited volume samples.

2.4 Effect of Age-dependent Vertical Diffusion

Since stars of different ages have different vertical scale heights, the observed value of \mathcal{R} depends on the volume within which the star counts are made. If the observed volume is a sphere of radius r_{obs} centered at the mid plane, then the ratio of stars of age t' that are within the sphere to the stars of the same age in a cylinder of the same radius but infinite z height is

$$F(t', r_{\text{obs}}) = \frac{\int_0^{r_{\text{obs}}} \left[1 - \left(\frac{z}{r_{\text{obs}}} \right)^2 \right] \exp \left[-\frac{z}{h(t')} \right] dz}{\int_0^{\infty} \exp \left[-\frac{z}{h(t')} \right] dz}, \quad (20)$$

$$= 1 - 2 \left[\frac{h(t')}{r_{\text{obs}}} \right]^2 + \frac{2h(t')}{r_{\text{obs}}} \left[1 + \frac{h(t')}{r_{\text{obs}}} \right] \exp \left[-\frac{r_{\text{obs}}}{h(t')} \right]. \quad (21)$$

Since the velocity dispersion of the stars increases with time, their scale height increases with age. We adopt

$$h(t') = \begin{cases} \sqrt{45^2 + (t'/0.0024 \text{ Gyr})^2} \text{ pc} & \text{if } 0 \leq t' \leq 0.5 \text{ Gyr} \\ 177(1+t')^{0.5} \text{ pc} & \text{if } t' > 0.5 \text{ Gyr} \end{cases} \quad (22)$$

the scale height for thin disk stars from Schröder & Pagel (2003).

Allowing for both (1) an exponentially declining SFR and (2) vertical diffusion, the ratio \mathcal{R}_{12} is given as

$$\mathcal{R}_{12}(r_{\text{obs}}, t_{\text{SFR}}, \Gamma) = \frac{\int_{1.5}^3 m^{-\Gamma} \left[\int_0^{\tau_{\text{MS}}(m)} F(t', r_{\text{obs}}) e^{t'/t_{\text{SFR}}} dt' \right] d \ln m}{\int_3^6 m^{-\Gamma} \left[\int_0^{\tau_{\text{MS}}(m)} F(t', r_{\text{obs}}) e^{t'/t_{\text{SFR}}} dt' \right] d \ln m}. \quad (23)$$

When $r_{\text{obs}} \rightarrow \infty$, we see from Equation (21) that $F(t, r_{\text{obs}}) \rightarrow 1$, as expected, so that the values of \mathcal{R}_{12} given by Equation (23) are the same as the values derived previously in Equation

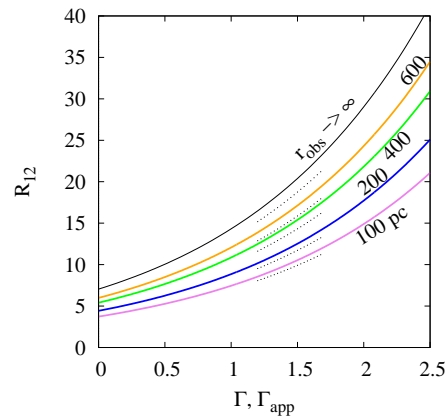


Figure 1. The ratio $\mathcal{R}_{12} \equiv \mathcal{N}_*(1.5 < m < 3) / \mathcal{N}_*(3 < m < 6)$ within a sphere of radius r_{obs} centered at the mid-plane as a function of the underlying IMF slope Γ when the star formation is uniform in the Galactic plane, exponential in the z direction, but age (and thus mass) dependent as given by Equation (22). The assumed SFH timescale is $t_{\text{SFR}} = 8.3$ Gyr for the solid lines and $t_{\text{SFR}} = \infty$ (constant SFR) for the dotted lines. The purple, blue, green and orange curves correspond respectively to the cases with $r_{\text{obs}} = 100, 200, 400$ and 600 pc. The black curve corresponds to the case $r_{\text{obs}} \rightarrow \infty$ where the effect of z -dispersion is irrelevant. In the latter case, \mathcal{R}_{12} reduces to \mathcal{R}_1 .

(14), where we assumed the stars of all masses well mixed. For example, with infinite r_{obs} and with $\Gamma = 1.35$, the \mathcal{R} values for $t_{\text{SFR}} = \infty$ and $t_{\text{SFR}} = 8.3$ Gyr are respectively $\mathcal{R} = 16.9$ and $\mathcal{R} = 18.6$. For finite values of r_{obs} the values of \mathcal{R} are reduced since $F(t, r_{\text{obs}})$ is smaller for the older (and therefore preferentially lower mass) stars with larger scale heights, fewer of which are captured in the observational volume.

Figure 1 shows the results from Equation (23) of varying the underlying Γ , the observational radius r_{obs} , and the SFH (t_{SFR}) on the ratio \mathcal{R}_{12} , the value of \mathcal{R} when both an exponentially declining average SFR and age-dependent vertical diffusion are taken into account. Correspondingly, for a given observed value of \mathcal{R} , the value of Γ inferred from this figure is $\Gamma_{\text{app},12}$. For simplicity, since we use this Figure 1 in

all the results reported in the next section, we reduce the notation to $\Gamma_{\text{app}} \equiv \Gamma_{\text{app},12}$. In this figure we plot two SFHs, $t_{\text{SFR}} = 8.3$ Gyr and $t_{\text{SFR}} = \infty$ (a constant SFR). The ratio \mathcal{R}_{12} increases with the steepness of the slope Γ , as expected. The main thing to notice is that the ratio \mathcal{R}_{12} decreases as r_{obs} decreases: Recall that the scale height of the stars with masses in the range $1.5\text{--}3 M_{\odot}$ (older stars) is larger than of the stars in the mass range $3\text{--}6 M_{\odot}$ (younger stars). Therefore, smaller observational volumes exclude a larger number of less massive stars, reducing \mathcal{R}_{12} . Hence the effect of vertical diffusion for finite r_{obs} is opposite to that of a declining SFR: a shrinking r_{obs} decreases \mathcal{R}_{12} , whereas a shrinking t_{SFR} increases \mathcal{R}_{12} .

There are two mechanisms which cause the observed ratio, and therefore the inferred $\Gamma_{\text{app},12}$, to vary in volumes sampled. (1) Statistical fluctuations (Poisson noise) cause minor changes due to finite volumes and therefore finite number of stars sampled. (2) Clustered star formation causes inhomogeneities in especially the high mass stars in the plane.

Figure 1 does not include the effect of statistical fluctuations of the number of stars within the observing volume. Even if we assume that star formation is uniform in the Galactic plane, these fluctuations cause variations of the ratio \mathcal{R} . However, for the average rate of star formation in the solar circle, these variations are negligible for $r_{\text{obs}} \geq 100$ pc since the number of stars within the volume are large. For example, about 1000 stars with masses in the range $3\text{--}6 M_{\odot}$ lie within $r_{\text{obs}} = 200$ pc, leading to a statistical variation of about 0.03 in the inferred $\Gamma_{\text{app},12}$. For $r_{\text{obs}} = 100$ pc the standard deviation of \mathcal{R} due to the clustering of the star formation process is more than four times larger than that due to the statistical fluctuations. Therefore, although it is strictly true that $\Gamma_{\text{app},12} = \Gamma$, the underlying slope of the universal IMF, only if $r_{\text{obs}} \rightarrow \infty$ so that spatial variations are averaged out, the statistical variations are sufficiently small that essentially $\Gamma_{\text{app},12} \simeq \Gamma$ for all observing radii greater than about 100 pc, *as long as the SFR is uniform in the Galactic plane*.

In the simulations we describe in the next section, the local SFR varies in both space and time (clustered star formation) so that the IMF slope $\Gamma_{\text{app},12}$ derived from the value of \mathcal{R}_{12} can be significantly different than the underlying Γ for finite volumes sampling the PDMF. In relating \mathcal{R}_{12} to $\Gamma_{\text{app},12}$, we have accounted for the effects of a non-constant SFH and the vertical diffusion, but not the effects of clustered star formation. The complicated modeling done by observers to infer Γ from PDMFs observed in finite local volumes of the Galaxy are quite analogous to this procedure: They are really measuring $\Gamma_{\text{app},12} \equiv \Gamma_{\text{app}}$ (assuming no observational errors and perfect assumptions on binarity, stellar atmospheres, interstellar extinction, etc) since they do not account for variations in the SFR in the plane of the Galaxy.

3 NUMERICAL SIMULATIONS OF THE PDMF FOR CLUSTERED STAR FORMATION

The goal of this section is to numerically model the formation of stars of mass $1.5 < m < 6$ in GMCs, and to follow their movement in time away from their birthsites to populate the

solar circle. In our simulations we input the SFH and the vertical diffusion so we can use the proper curve on Figure 1 to obtain Γ_{app} , which differs from Γ due to spatial variations in stellar densities, particularly of the higher mass stars, as well as the statistics of small numbers of such stars in small volumes. We numerically compute the densities of stars of mass $1.5 < m < 6$, evaluate \mathcal{R} in small volumes in the simulations, and then use Figure 1 to account for the SFH and the vertical segregation to derive Γ_{app} , the value observers would infer based on their assumption that star formation is not clustered. With many simulations, we obtain the probability distribution of Γ_{app} for a given volume sampled. We also look at the effect of the Sun's location in an interarm region of the solar circle in the following section.

3.1 Model

3.1.1 Summary of Basic Model

In order to determine the effect of spatial and temporal fluctuations in the SFR on the PDMF, we model a large volume around the solar circle in a frame that moves with the galactic rotation at the solar circle. The x, y coordinates are in the plane and cover 25 and 1.5 kpc respectively, with the 25 kpc representing about one half of the solar circle and the 1.5 kpc the radial extent of the model. GMCs form randomly (or concentrated in spiral arms) along the solar circle and live for 20 Myr. The stars are born in GMCs during the GMC lifetime and given random velocities in the plane. We follow the motion of the stars in the Galactic plane for 2.57 Gyr, since our least massive star considered, $m = 1.5$, has this lifetime. At the end of the simulation $\sim 2.4 \times 10^7$ stars (all with masses in the range $m = 1.5\text{--}6$) have been formed in the simulation area but only $\sim 8 \times 10^6$ remain on the main sequence. These main sequence stars are distributed in the simulation volume in z with an age dependent scale height given by Equation (22). We then compute ratios \mathcal{R}_{12} in many small volumes centered on the midplane of the Galaxy at the solar circle, and from these many volumes, and a large number of independent simulations, use the distribution of \mathcal{R}_{12} to determine the distribution of Γ_{app} from Figure 1 for a range of values of the underlying Γ . For the convenience of the reader we present here Table 2 that lists the parameters used in the simulations, identifies which were fixed and which were varied, and specifies the values or value range of these parameters.

3.1.2 Formation and Distribution of GMCs

The clustering of star formation events in space and time is driven by the fact that much of the mass in GMCs, where stars form, is concentrated in the most massive clouds (Williams & McKee 1997; Heyer & Dame 2015). We refer the reader to Hennebelle & Falgarone (2012) for a review of the physics of molecular clouds and of their formation.

For our standard case we adopt the GMC model of Williams & McKee (1997) (hereafter WM97), with one important exception: Miville-Deschênes et al. (2017) have shown that the surface density of the molecular gas in the Galaxy scales as $\exp(-R/H_R)$ with $H_R = 2$ kpc, significantly less than the 3.5 kpc estimated by WM97. Miville-Deschênes et al. (2017) found that this distribution

Table 2. Model Parameters and their Values

	Description	Standard Value	Alternative Values
r_{obs}	Radius of observed volume.	200 pc	100, 400, 600, 750 pc
Star Formation			
SFR	Star Formation Rate in $3 \leq R_G \leq 11$ kpc.	$1.6 M_{\odot}/\text{yr}$	
R_{\odot}	Galactic radius of the solar circle.	8.3 kpc	
H_R	Radial scale length of stars and gas.	2.0 kpc	
t_{SFR}	Global SFR decay time.	8.3 Gyr	∞
Initial Mass Function of individual stars			
Γ	– Slope of the underlying high mass IMF.	$1.2 \leq \Gamma \leq 1.7$	
C	IMF normalization constant ($0.004 < m < 120$). See eq. 2	$C(\Gamma = 1.35) = 0.108$	
GMC properties			
τ_{GMC}	Lifetime of GMCs.	20 Myr	
\mathcal{N}_{cu}	See eq. 24.	63	38^a
γ_c	– Slope of the GMC mass distribution.	0.6	$0.6^a, \text{M17}^b$
(M_l, M_u)	Lower and upper mass limits of GMCs.	$(10^5, 6 \times 10^6) M_{\odot}$	$(10^5, 10^7) M_{\odot}^{a,b}$
Stellar Dispersion			
$h(\tau)$	Vertical scale length of stars of age τ .	see eq. 22	
$\sigma_{\text{ABS}}(\tau)$	In-plane velocity dispersion of stars with ages $\tau \geq 500$ Myr.	see eq. A.1	
σ_{min}	In-plane velocity dispersion of stars at birth.	6 km s^{-1}	
$\sigma(\tau)$	In-plane velocity dispersion of stars of age τ .	see eq. A.2	$\sigma_{\text{min}}, \sigma_{\text{ABS}}$
Properties of spiral arms			
N_S, N_W	number of strong and weak spiral arms.	2, 2	
F_S, F_W	Fraction of GMCs formed in the strong and weak arms.	$1/2, 1/5$	$1/3, 1/6$
α	Pitch angle of spiral arms.	12° .	
Δ_a	Full arm width measured normal to the arm.	0.8 kpc	
v_a	Arm velocity with respect to the LSR.	-50 km s^{-1}	

^a Truncated power-law in [Rice et al. \(2016\)](#).
^b PDF for inner Galaxy clouds in [Miville-Deschênes et al. \(2017\)](#).

extends from 4 to 17 kpc. In order to approximately include the molecular gas inside 4 kpc, we extend the exponential in to 3 kpc and assume that the density of molecular gas inside that is negligible. The mass of molecular gas inside the solar circle, including He, is about $1.0 \times 10^9 M_{\odot}$ ($\pm 30\%$) according to [Heyer & Dame \(2015\)](#), just as estimated by WM97. In our model GMCs are created following a truncated power-law mass distribution:

$$\frac{d\mathcal{N}_c(M)}{d\ln M} = \mathcal{N}_{\text{cu}} \left(\frac{M_u}{M} \right)^{\gamma_c} \quad (M_l \leq M \leq M_u), \quad (24)$$

where $d\mathcal{N}_c/d\ln M$ represents the mass distribution of all the GMCs inside the solar circle. In our standard case we assume the WM97 parameter values $M_u = 6 \times 10^6 M_{\odot}$, $\mathcal{N}_{\text{cu}} = 63$ and $\gamma_c = 0.6$, and assume that the actively star forming clouds have masses over $M_l = 10^5 M_{\odot}$ which contain 80% of the molecular mass. The mass distribution of GMCs is somewhat uncertain, and we discuss in Section 3.2.3 below the variation in the literature of the parameters γ_c , M_u , \mathcal{N}_{cu} , test several other mass distributions, and determine the effect of these uncertainties on the determination of Γ_{app} . Because most of the mass is in the largest clouds ($\gamma_c < 1$), the results are insensitive to the value of M_l .

We represent the radial distribution of the GMCs as

$$\frac{d^2 \mathcal{N}_c(M)}{dA d\ln M} = \frac{e^{(R_0-R)/H_R}}{A_{\text{eff}}} \frac{d\mathcal{N}_c(M)}{d\ln M}, \quad (25)$$

where $R_0 = 8.3$ kpc is the radius of the solar circle and

$$A_{\text{eff}} = 2\pi H_R^2 \left[\left(1 + \frac{R_i}{H_R} \right) e^{(R_0-R_i)/H_R} - \left(1 + \frac{R_0}{H_R} \right) \right], \quad (26)$$

where R_i is the inner radius of the distribution; this differs by a factor $\exp(R_0/H_R)$ from the expression in [McKee & Williams \(1997\)](#). For our adopted parameters ($H_R = 2$ kpc, $R_i = 3$ kpc, and $R_0 = 8.3$ kpc), we have $A_{\text{eff}} = 760 \text{ kpc}^2$. There are about 200 clouds more massive than $10^6 M_{\odot}$ inside the solar circle, containing about half the total mass of molecular gas; this corresponds to a surface density of $200/A_{\text{eff}} = 0.26 \text{ GMCs kpc}^{-2}$. We assume that GMCs make stars for a period of 20 Myr ([Blaauw 1991](#)), which we adopt as their lifetime. The typical star in the mass range $m = 3 - 6$ has a lifetime of about 200 Myr (weighted by the PDMF) and therefore an observed age of about 100 Myr. In that time, the total number of $M > 10^6 M_{\odot}$ GMCs that would be born is about $(100/20) \times 0.26 \text{ kpc}^{-2} = 1.3 \text{ kpc}^{-2}$. The mean distance between these associations is about 1 kpc. Since this is the distance that a star can travel in 100 Myr at a typical velocity dispersion of 10 km s^{-1} , we expect significant inhomogeneity in the surface distribution of

these stars. Recall from the discussion in Section 2.2 that a decrease in the number of $m = 3 - 6$ stars relative to the number of $m = 1.5 - 3$ stars by 36% could alter the inferred Γ_{app} from 1.35 to 2. As a result, we expect significant effects from the inclusion of clustering of star formation.

We simulate clouds with masses exceeding $10^5 M_{\odot}$, which contain 80% of the mass; their surface density is 1.5 kpc^{-2} . We assume that the formation rate of GMCs is proportional to the SFR; hence, for a SFR that declines with time as $\exp(-t/t_{\text{SFR}})$, the number of GMCs grows with look back time as $\exp(t'/t_{\text{SFR}})$. We adopt $t_{\text{SFR}} = 8.3 \text{ Gyr}$, so that about 10000 are formed in the 37.5 kpc^2 simulation area during 3 Gyr, but only 1800 of them have masses above $10^6 M_{\odot}$. In the standard case the placement of the GMCs is random in the x, y plane and at $z = 0$, but in Section 4 we consider the effect of spiral waves in concentrating the population of GMCs. The scale height of GMCs is small ($\sim 60 \text{ pc}$ —Heyer & Dame 2015) compared to the scale heights that the stars attain after traveling through the ISM, so that the assumption of $z = 0$ is justified.

3.1.3 Star Formation in GMCs

Stars are formed in the GMCs at a constant rate so that over the GMC lifetime a fraction f_e of the mass M of a particular cloud is converted into stars. The average current rate of star formation in the Galaxy is $\simeq 1.6 M_{\odot}/\text{yr}$ (Chomiuk & Povich 2011, Lee et al 2012). Assuming that the SFR scales with the surface density of GMCs, we compute that within the solar circle the star formation rate is $1.44 M_{\odot}\text{yr}^{-1}$. Comparing this to the molecular mass $7.6 \times 10^8 M_{\odot}$ in this region and utilizing the fact that GMCs lifetimes are 20 Myr, we find the average efficiency of star formation is $f_e \simeq 0.038$. For simplicity we assume that the star formation efficiency is constant over the mass range 10^5 to $6 \times 10^6 M_{\odot}$, and we neglect star formation in lower mass clouds. We have made simulations where for each GMC we allow for 1/2 standard deviation around the average star formation efficiency, and find that the results for the Γ_{app} distribution have only minimal changes. Although we form stars at random positions in the GMCs, the placement is not important since GMCs are very small compared to the interstellar volume over which we average.

The stellar mass distribution in each star forming event is set by a fixed Γ for $m > 1.5$, and we focus on stars of mass $m = 1.5 - 6$. We have run simulations with $\Gamma = 1.2, 1.35, 1.5$ and 1.7 . We find (see Sec. 3.2.1 below) that if we plot the distribution of $\Delta\Gamma_{\text{app}} \equiv \Gamma_{\text{app}} - \Gamma$, the results do not depend on Γ in this range. Therefore, we present our results in terms of the distribution of $\Delta\Gamma_{\text{app}}$, the deviation of Γ_{app} from the underlying Γ .

3.1.4 Stellar Dispersal from GMCs into the ISM

The effect of stellar clustering on the inferred IMF depends critically on the rate at which stars move from their birth sites. We describe our method for determining the final location of each star in the Galactic plane in Appendix A. We use data from Nordström et al. (2004) and Dehnen & Binney (1998) to fit the time-dependent expression for stellar velocity dispersions given by Aumer et al. (2016) for ages τ

greater than 0.5 Gyr. For our standard expression, we linearly interpolate from an initial dispersion of 6 km s^{-1} (Aumer et al. 2016) to the values at 0.5 Gyr. Each star is then given a velocity drawn at random from a Gaussian distribution with a dispersion equal to the time-averaged dispersion for a star of that age, and its final position is determined. To gauge the effects of uncertainties in the velocity dispersion, we also consider an upper limit on the dispersion given by using the Aumer et al. (2016) expression for $\tau < 0.5 \text{ Gyr}$ and a lower limit given by setting the dispersion equal to its initial value, 6 km s^{-1} . If the stars encounter a boundary in the simulation during their lifetime, we adopt periodic boundary conditions to recover the stars that leave the simulation area (see Appendix A). At the end of the simulation (at 3 Gyr) the stars are distributed in z with the age dependent scale height given by Equation (22). At this time we know the x, y, z position and mass of each star in our simulation volume.

3.1.5 Determination of the Probability Distribution of Γ_{app}

Knowing the position and mass of each star, we then place small (compared with the simulation size) spherical volumes of radius r_{obs} , based on observational limits, within each simulation, and run numerous simulations to add to the statistics. Inside the volumes of radius r_{obs} we determine \mathcal{R} by counting the stars in the mass range $m = 1.5 - 3$ and rationing that number with the number of stars with $m = 3 - 6$. Since we have included the SFH and vertical diffusion in the simulation, this value of \mathcal{R} is \mathcal{R}_{12} , and we can use the appropriate curve in Figure 1 to infer Γ_{app} . This value of Γ_{app} differs from the underlying Γ only because of inhomogeneities in the relative densities of low- and high-mass stars. These inhomogeneities are mainly caused by the fact that the shorter-lived, high mass stars do not move rapidly enough from their localized birthsites (GMCs) in their lifetimes to uniformly populate the Galactic plane. Each volume then can have an excess or a deficit of massive stars relative to low mass stars, and there is therefore a range of values of Γ_{app} even though Γ is fixed. In what follows, we examine the dependence of the distribution of values of $\Delta\Gamma_{\text{app}} = \Gamma_{\text{app}} - \Gamma$ on the observational volume, the underlying Γ , the dispersion speed of the stars, and the initial spatial concentration of the stars. We also examine the effect of spiral density waves on the distribution of the GMCs, and the subsequent distribution of $\Delta\Gamma_{\text{app}}$.

3.1.6 Uncertainties in the Simulations

We emphasize that our simulations should be considered as examples, and not a precise representation of conditions at the solar circle. We have chosen plausible parameters and have endeavored to obtain a good estimate of the inhomogeneous distribution of stars in the plane of the Galaxy, and of the variations in the SFR per unit volume as a function of position along the solar circle. However, there are many uncertainties: The mass distribution of GMCs, their lifetimes, and the star formation efficiencies inside GMCs with different masses are all uncertain. The velocity distribution of newly formed stars as a function of time is uncertain, as they proceed from the random velocities incurred during their formation in GMCs to the velocities they achieve after many

gravitational encounters with molecular clouds. In our initial model we assume that GMCs form at random positions in the plane. However, in Section 4 we describe the possible effects caused by spiral arms. This treatment is also exemplary, because the number and strength (i.e., the ratio of the SFR per unit area in the arms versus that in the inter-arm) of these arms is uncertain, as is the exact position of the Sun with respect to these arms. Probably the two most significant uncertainties are the mass distribution of GMCs and the effect of spiral arms in affecting the spatial distribution of GMCs. We test the effect of these uncertainties in Sections 3.2.3 and 4 below.

3.2 Results

In all the results presented below, we carried out 360 simulations in which we placed 25 independent observing spheres of radius r_{obs} (our standard value is $r_{\text{obs}} = 200$ pc but we present cases where the radius is varied) centered in the mid-plane and separated by 1 kpc, providing 9000 different independent values of $\Delta\Gamma_{\text{app}}$. The standard of 200 pc is chosen because both Dawson & Schöder (2010) and Rybizki & Just (2015) use observations samples with $r_{\text{obs}} = 100 - 200$ pc. However, Czekaj et al (2014) use a sample with apparent magnitude up to $V=11$, which corresponds to a distance of about 300-400 pc for the lower mass stars in our sample. Therefore, we include analysis up to $r_{\text{obs}} = 600$ pc in this section and even larger in the next section. Note that our simulation uses volume limited samples, not magnitude limited samples.

All the results presented in this paper are for observational spherical volumes centered at the mid-plane. Off plane results require a reevaluation of $F(t', r_{\text{obs}})$ to infer Γ_{app} from the value of R within an off-plane sphere (i.e. a new Figure 1). However, if the sphere is placed at a distance above the plane that is small compared to r_{obs} and to the scale height of high-mass stars, one expects negligible differences compared to the results obtained with the spheres centered in the mid-plane. The Sun is located about 15-25 pc above the mid-plane (Drimmel & Spergel 2001), a distance that is small compared to r_{obs} and to the scale height of high-mass stars, both larger than 100 pc. Therefore we ignore this effect in the simulations that follow.

In this section, we form GMCs at random positions around the solar circle. In Section 4 we treat GMCs forming preferentially in spiral arms.

3.2.1 Probability of finding $\Delta\Gamma_{\text{app}} \geq +.35$ for $r_{\text{obs}} = 200$ pc, independent of Γ

Figure 2 shows the probability distribution of the inferred $\Delta\Gamma_{\text{app}}$ for four different values of Γ . For the case under consideration ($r_{\text{obs}} = 200$ pc), the mean and median value of $\Delta\Gamma_{\text{app}}$ are about +0.1 and the dispersion is about $\sigma \simeq 0.45$. In other words, the inhomogeneous distribution of stars resulting from clustered star formation as described in Section 3.1.2 causes the inferred Γ_{app} to be typically about 0.1 higher than the underlying Γ . This conclusion should depend only weakly on the parameters we have adopted for the SFH ($t_{\text{SFR}} = 8.3$ Gyr) and stellar scale heights given in Equation (22) since they are accounted for in our relation between

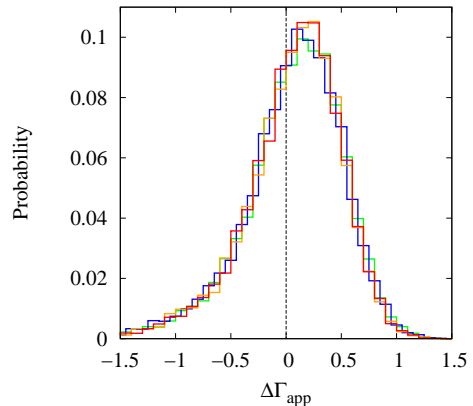


Figure 2. Probability distribution of $\Delta\Gamma_{\text{app}}$ for four different values of the underlying Γ . Green is $\Gamma = 1.2$, blue is $\Gamma = 1.35$, orange is $\Gamma = 1.5$, and red is $\Gamma = 1.7$. The bin size is $\Delta\Gamma_{\text{app}} = 0.05$. The plots are essentially the same, showing that probability distribution of $\Delta\Gamma_{\text{app}}$ does not depend on Γ . We assume here the standard stellar random velocity distribution and $r_{\text{obs}} = 200$ pc.

the “observed” \mathcal{R} and the inferred Γ_{app} —there would be no dependence in the absence of clustered star formation, since then $\Gamma_{\text{app}} = \Gamma$, ignoring the small statistical fluctuations due to finite sample size.

In addition, we can estimate the likelihood that $\Delta\Gamma_{\text{app}}$ is greater than any fixed value. For example, the probability that $\Delta\Gamma_{\text{app}} > 0.35$ – i.e., probability that the observer/modeler obtains $\Gamma_{f,\text{app}} > 1.7$, when in fact the underlying $\Gamma = 1.35$ – is $\sim 30\%$. We shall discuss the effect of spiral arms below, but in the absence of their effect, these results suggest that the observation of $\Gamma_{\text{app}} \simeq 1.7 - 2.1$ favors a somewhat higher value of Γ than 1.35, although there still is a significant possibility that $\Gamma = 1.35$.

Finally, we find that the distribution of values of Γ_{app} is independent of the underlying slope, Γ . In the rest of this section, we therefore present results as functions of $\Delta\Gamma_{\text{app}}$.

3.2.2 Dependence of $\Delta\Gamma_{\text{app}}$ on the Stellar Velocity Dispersion

Before proceeding further, it is important to show that our results are not very sensitive to the velocity dispersion, as long as the values remain in reasonable bounds. Figure 3 presents three representations of the time dependent velocity dispersions of the stars for the case where $r_{\text{obs}} = 200$ pc (see Appendix A for details of our treatment of velocity dispersion). Stars are accelerated from their initial random speeds by gravitational forces in the Galactic plane (e.g., passage of spiral arms or encounters with GMCs). Therefore, the minimum velocity dispersion of a star would be to hold the dispersion constant in time with the initial dispersion, which we have taken to be 6 km s^{-1} from Aumer et al. (2016). We take the time-dependent velocity dispersion given by Aumer et al. (2016), $\sigma_{\text{ABS}}(\tau)$, to be the maximum since it is observed to be too large at early times—the radial velocity at $\tau = 0$ is more than twice the observed value (see Appendix A). The standard velocity distribution is intermediate between the minimum and maximum dispersions, with the velocity dispersion increasing linearly with τ from the lower

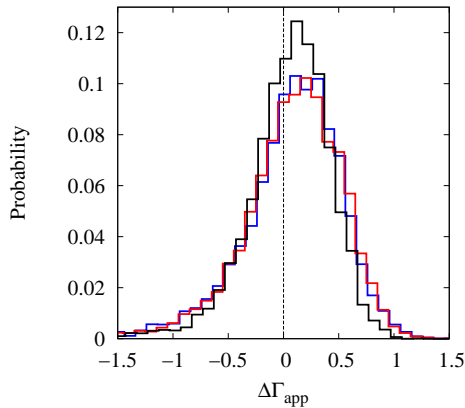


Figure 3. Distribution of $\Delta\Gamma_{\text{app}}$ for our three velocity dispersions of stars, assuming $r_{\text{obs}} = 200$ pc. Red is the minimum dispersion of 6 km s^{-1} in U and V. Black is the maximum dispersion as given in Aumer et al. (2016; see text). Blue plots the probability distribution for the standard case, in which the velocity dispersion linearly increases from 6 km s^{-1} to the Aumer et al. (2016) result during the first 500 Myr.

to the upper limit during the first 500 Myr and matching $\sigma_{\text{ABS}}(\tau)$ thereafter. As expected, the minimum velocity dispersion has a slightly broader probability distribution as a function of $\Delta\Gamma_{\text{app}}$, since the slower stars maintain a larger spatial inhomogeneity. However, the difference between the three cases is small because the random stellar speeds ($\sim 10 \text{ km s}^{-1}$) in all three cases are quite similar. In addition, recall that GMCs are forming at random positions constantly to replace GMC that have died. This places stars more uniformly in the Galactic plane than if the sites of star formation were frozen in time. Figure 3 shows that our results are not sensitive to the standard velocity dispersion we have chosen. The overall conclusion is that for reasonable values of the velocity distribution of the stars, migration is not enough to eliminate the effect of the clumpy nature of the star formation process.

3.2.3 Dependence of $\Delta\Gamma_{\text{app}}$ on the Concentration of GMCs

We next examine the dependence on the concentration of star formation events. The distribution by mass of GMCs is uncertain, and there have been several studies in the recent literature with somewhat different results. Clouds outside the solar circle are smaller than those at or inside the solar circle (Heyer & Dame 2015), so we focus on the latter. The data used by WM97 (e.g., Solomon et al. 1987) assigned only 40% of the molecular gas to clouds, and WM97 then assumed that the remaining 60% was in clouds of the same mass distribution, but were too cold to appear in the catalogs. We note as justification that locally all the molecular gas is in clouds. Subsequently, Rosolowsky (2005) found $\gamma_c = 0.53$, $N_{\text{cu}}/\gamma_c = 27 - 36$, and $M_u = (3 - 4) \times 10^6 M_\odot$ based on the data of Solomon et al. 1987, whereas Rice et al. (2016) found $\gamma_c = 0.6 \pm 0.1$, $N_{\text{cu}}/\gamma_c = 11 \pm 6$, and $M_u = (1.0 \pm 0.2) \times 10^7 M_\odot$. These parameters were introduced and discussed in Section 3.1.1 above. (Note that these workers assign only a fraction of the molecular mass to clouds, whereas WM97 assumed it was all in clouds.) On the other hand,

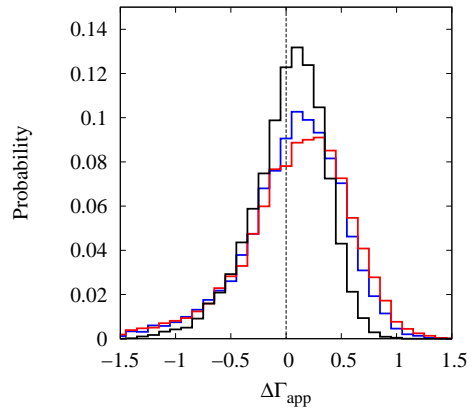


Figure 4. Probability distribution of the deviation $\Delta\Gamma_{\text{app}}$ from the underlying IMF slope for three different concentrations of the star formation events, corresponding to three different mass distributions of GMCs. The blue histogram corresponds to our standard case, where the mass distribution is from WM97. The red curve corresponds to the mass distribution of Rice et al (2016, see text). This distribution has more molecular mass in fewer, larger GMCs and therefore is the most concentrated and results in the broadest distribution in $\Delta\Gamma_{\text{app}}$ as expected. On the other hand, the Miville-Deschênes et al. (2017) distribution puts mass into a greater number of clouds, leading to a narrower distribution in $\Delta\Gamma_{\text{app}}$ (black curve). Other parameters are $r_{\text{obs}} = 200$ pc and standard velocity distribution.

Miville-Deschênes et al. (2017) did not find a cutoff distribution, but instead found $\gamma_c = 2$ at very high masses; furthermore, they assigned 98% of the CO emission to clouds. One thing all these distributions have in common is that most of the molecular mass in the distribution is concentrated in the most massive clouds, which are not abundant and are therefore widely spaced. Hence, if all the molecular mass is assigned to these cloud distributions, then the results will not differ significantly from our standard model using WM97. We show in Figure 4 the effect of these different GMC distributions on $\Delta\Gamma_{\text{app}}$ when all the molecular mass is assigned to these distributions. If the $\sim 60\%$ of the CO emission not assigned to clouds by Solomon et al. (1987), for example, is in more diffuse clouds that are not actively forming stars, then there would be even fewer star-forming clouds than in our standard WM97 model, and the more widely dispersed sites of star formation would produce greater deviations in Γ_{app} from Γ .

Figure 4 shows the expected broader distribution in $\Delta\Gamma_{\text{app}}$ when stars form in more concentrated spatial locations (Rice et al. 2016 case) compared to the Miville-Deschênes et al. (2017) case which distributes the mass in a greater number of smaller clouds. More localized birth sites lead to a final stellar spatial distribution that is much more inhomogeneous (especially for the shorter-lived high-mass stars), and thus the inferred $\Delta\Gamma_{\text{app}}$ shows a broader distribution and, as noted above, a shift ($\sim +0.1$) toward positive values (that is, Γ_{app} greater than the underlying Γ). Although not evident in Figure 4, the narrowing of the distribution in the Miville-Deschênes et al. (2017) case has a significant effect on the probability that $\Delta\Gamma_{\text{app}} > 0.35$, or, in other words, that $\Gamma_{\text{app}} > 1.7$ when the

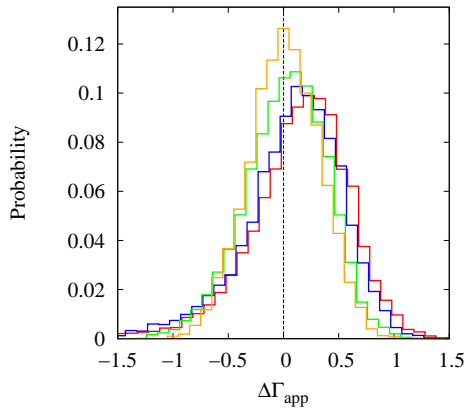


Figure 5. Probability distribution of $\Delta\Gamma_{\text{app}}$ as a function of observing volume. The red, blue, green and orange curves correspond to the cases when the ratio \mathcal{R} is measured within a sphere of radius 100, 200, 400 and 600 pc respectively. As expected, as r_{obs} increases the distribution narrows around $\Delta\Gamma_{\text{app}} = 0$, i.e., Γ_{app} approaches Γ .

underlying $\Gamma = 1.35$. Assuming $\Gamma = 1.35$, the WM97 case, the Rice et al. (2016) case and the Miville-Deschênes et al. (2017) case have the following probabilities that $\Gamma_{\text{app}} > 1.7$: 0.27, 0.31, and 0.15. We therefore conclude that the uncertain distribution of GMCs by mass leads to a $\sim 15 - 30\%$ chance that $\Delta\Gamma_{\text{app}} > 0.35$ if GMCs are formed randomly in the plane of the solar circle.

3.2.4 Dependence of $\Delta\Gamma_{\text{app}}$ on Observing Volume

Figure 5 shows the dependence of the probability distribution of $\Delta\Gamma_{\text{app}}$ on the observing volume for the standard case with the standard velocity distribution. Recall that our approach, using Figure 1 to determine $\Delta\Gamma_{\text{app}}$ from the ratio \mathcal{R} , has corrected for the vertical differences in massive and low mass stars as well as the SFH. Therefore, the narrowing of the distribution and the shift to an average value $\Delta\Gamma_{\text{app}} \simeq 0$ as r_{obs} increases is solely due to the larger volumes averaging out the x, y spatial inhomogeneities of the more massive stars. The mean and median values of $\Delta\Gamma_{\text{app}}$ for the cases corresponding to $r_{\text{obs}} = 100, 200, 400$ and 600 pc are respectively (0.13, 0.17), (0.09, 0.13), (0.02, 0.04) and (0.02, 0.02). This demonstrates that the effect of inhomogeneity systematically increases Γ_{app} above the underlying Γ as the observing volume shrinks. The percentage of simulations with $\Delta\Gamma_{\text{app}}$ in the range -0.15 to $+0.15$ are respectively 24%, 26%, 30% and 34%. The percentages of simulations with $\Delta\Gamma_{\text{app}} > 0.35$ (so that, for example, measures of $\Gamma_{f,\text{app}} > 1.7$ actually correspond to an underlying $\Gamma = 1.35$) are 33%, 30%, 20%, and 17%. Thus, for example, with $r_{\text{obs}} = 200$ pc it is more likely to infer $\Gamma_{\text{app}} > \Gamma + 0.35$ than it is to infer that Γ_{app} lies within ± 0.15 of Γ . In another interesting example of these results, for a volume sample of $r_{\text{obs}} = 200$ pc with random placement of the Sun along the solar circle (ignoring the effects of spiral density waves), the chances of inferring $\Delta\Gamma_{\text{app}}$ within ± 0.25 of the underlying Γ (42%) is similar to the probability of inferring $\Delta\Gamma_{\text{app}} > 0.25$ (43%).

The most important features in Figures 2-5 are: (i) the broad dispersion in $\Delta\Gamma_{\text{app}}$ which is the main point of this

paper, (ii) the shift in $\Delta\Gamma_{\text{app}}$ toward positive values (i.e., Γ_{app} larger and thus a steeper apparent IMF), and (iii) an asymmetry between negative and positive values with a long tail on the negative side (cases with a flatter IMF and more massive stars). The shift to positive values of $\Delta\Gamma_{\text{app}}$ is due to the short lifetimes of massive stars and the low space density of young star forming regions. Most of space has a deficit of massive stars compared to the density these stars would have if star formation were homogeneous in space. Therefore, for a fixed observing volume, there is greater chance of being in a region of deficit than of excess of massive stars. Similarly, the tail on the negative side is created by those few volumes that fall around active star formation regions. Both the shift and the asymmetry decrease as the observing volume increases, because larger volumes encompass both regions of deficit and excess.

The standard deviations of the $\Delta\Gamma_{\text{app}}$ distributions decrease only moderately as r_{obs} increases from 100 to 600 pc (from 0.45 to 0.32).³ The modest amount of narrowing with observing radius might seem surprising, but recall that most stars form in the largest GMCs that are ~ 1 kpc apart, and that a significant fraction have slow diffusion speeds so that significant variations can still occur on the 600 pc scale. In addition, the distribution depends on the local star formation history in the general location of the observing volume. Although the *average* SFH at the solar circle declines somewhat in our standard case over the last 3 Gyr, the localized nature of star formation means that there are significant fluctuations in the SFR over smaller volumes and over timescales of order the lifetime (~ 100 Myr) of the massive $m = 3 - 6$ stars. We study these temporal fluctuations next.

3.2.5 Fluctuations in the SFR Over Small Volumes

Elmegreen & Scalo (2006) have discussed the effect of peaks and lulls in the SFR on the inference of the high mass IMF from the PDMF. For example, if a region has suffered a lull over the past 100 Myr, there will be a deficit of short-lived, massive stars and the inferred slope of the high mass IMF will be steeper. Figure 6 displays the fluctuations in the star formation rate $\langle \text{SFR} \rangle_{100\text{Myr}}$ averaged over the previous 100 Myr. If the SFR is averaged over the entire 30 kpc^2 area of the simulation (red curve), we see that the fluctuations are not large. However, when the SFR is averaged over smaller 1.2 kpc^2 areas, the SFR changes significantly over ~ 100 Myr timescales. Note that the black and orange curves fall significantly below the global average SFR whereas the green curve falls significantly above the global average. The underproduction of $m = 3$ stars in the black and orange cases should lead to a higher value of Γ_{app} whereas the overproduction seen in the green case should lead to a low value of Γ_{app} compared to the underlying Γ . In fact, in this particular simulation where we have chosen an underlying $\Gamma = 1.35$ the values of the ratio \mathcal{R} within 600 pc from the points at $x=4.5$ (green), 9.5 (black) and 16.5 (orange) kpc at t_0

³ The standard deviations of the $\Delta\Gamma_{\text{app}}$ distribution continue to decrease as the sampled region increases, reaching the value of 0.05 for the whole simulation area.

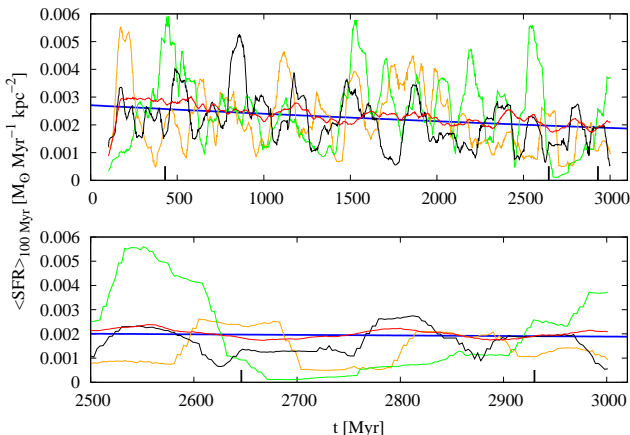


Figure 6. Evolution of the star formation rate averaged over the previous 100 Myr, $\langle \text{SFR} \rangle_{100 \text{ Myr}}$, for a particular simulation. As in all simulations, stars form in widely spaced GMCs. The current epoch is $t \equiv t_0 = 3000$ Myr. The lower panel is an expanded version of the upper panel for the last 500 Myr. The vertical ticks on the x-axis indicate the survival times (MS stellar lifetimes) into the past for stars of 1.5, 3 and 6 M_{\odot} . The red curve corresponds to the $\langle \text{SFR} \rangle_{100 \text{ Myr}}$ occurring in the whole simulation area ($0 < x < 25$ kpc and $0 < y < 1.2$ kpc). The green, black and orange curves correspond to the $\langle \text{SFR} \rangle_{100 \text{ Myr}}$ in three 1.2 kpc² regions of the simulation area, respectively in the x-axis sections 4-5 kpc, 9-10 kpc and 16-17 kpc. The blue curve corresponds to the smooth average evolution of the SFR at the solar circle, or $\text{SFR} = \text{SFR}(t_0) e^{t'/\tau_{\text{SFR}}}$ where $t' \equiv t_0 - t$ is the look back time in Gyr. The simulation parameters are $\tau_{\text{SFR}} = 8.33$ Gyr and standard velocity dispersion.

are respectively 11.7 ($\Gamma_{\text{app}}=0.96$), 21.6 ($\Gamma_{\text{app}}=1.83$) and 21.5 ($\Gamma_{\text{app}}=1.82$), in accordance with the above prediction.

4 EFFECT OF SPIRAL ARMS ON THE PDMF

If the Sun were located in a random position at the solar circle, we would then conclude from the above simulations that observations with a limited observing volume would have a roughly 15-35% chance of finding $\Gamma_{\text{app}} \simeq 1.7 - 2.1$ if the underlying $\Gamma = 1.35$. However, the Sun is not at a random position: it currently resides in an interarm region where the star formation rate is low, and as a result the PDMF is altered in such a way as to suggest a steeper IMF (Elmegreen & Scalo 2006; in our terminology, this leads to a positive $\Delta\Gamma_{\text{app}}$). As first noted by Drimmel & Spergel (2001), observations of near- and mid-IR stellar tracers indicate the presence of only two spiral arms. However, observations of the gas and dust in the radio and far-IR indicate four arms (e.g., Georgelin & Georgelin 1976; Koo et al. 2017). We therefore follow Benjamin (2008) and Robitaille et al. (2012) and assume that there are two strong arms and two weak ones. The Sun has left the weak Sagittarius-Carina arm and will encounter the strong Perseus arm. In our spiral arm model we include star formation that occurs in the interarm region but with a lower intensity than in the strong and weak arms. We neglect the Orion Spur, a minor arm that crosses the region where the Sun is located (Drimmel et al. 2003), and consider it as part of the low intensity star formation that occurs in the interarm region of our model. As discussed in

Appendix B, the speed of the arms with respect to the Local Standard of Rest (LSR) is about -50 km s⁻¹; with 4 arms, this implies that the solar neighborhood is overtaken by an arm every ~ 260 Myr. However, due to the finite width of the arms and the small pitch angle (see Appendix B) the time spent in the interarm region is reduced to ~ 180 Myr. The star formation rate per unit area is larger in the arms than in the interarm regions, so the Sun has experienced a relatively low star formation rate for ~ 90 Myr preceded by a higher rate when the Sun lay in an arm. The lower mass stars ($m \sim 1.5$) live long enough to diffuse through the solar circle and therefore have a relatively uniform population when comparing arm and interarm. However, the higher mass stars ($m > 3$) have shorter lives and are more concentrated in the arms, which leads to larger values of Γ_{app} in the interarm region compared to the underlying Γ .

To consider the effect of the spiral arms, the only change we make is to assume that the probability of formation of GMCs is enhanced in the arm regions. We fix this enhancement by the fraction, F_S , of the GMCs that are formed in the two strong arm regions and the fraction, F_W , of GMCs formed in the two weak arm regions. The properties of the spiral arm model that we adopt are described in Appendix B: the number of arms, 4, the star formation fractions, $F_S = 0.5$ and $F_W = 0.2$, the pitch angle $\alpha = 12^\circ$, the arm width normal to the arm, $\Delta_a = 0.8$ kpc, and the arm velocity with respect to the LSR, $v_a = -50$ km s⁻¹, as noted above. Note that the thickness of the arm along a circular orbit is $\Delta_x = \Delta_a / \sin \alpha = 3.8$ kpc. The key parameter in considering the effect of spiral arms is $F_I \equiv 1 - F_S - F_W$, the fraction of GMC formation in the interarms. As discussed in Appendix B, observations of external galaxies suggest that the range of F_I is 0.1-0.6. For our standard case mentioned above, we take $F_I = 0.3$, but we also treat a case with $F_I = 0.5$. Smaller values of F_I lead to more suppression of the SFR in the interarm over the past ~ 90 Myr, and thus a larger value of Γ_{app} .

Figure 7 shows the effect of the modulation of the SFR due to the spiral wave passage for the standard spiral arm case described above ($F_I = 0.3$). These parameters imply that the relation of the star formation rate per unit area in the strong-arm, weak-arm and interarm regions is respectively 8:3:1. The results shown correspond to 360 simulations done for the same set of parameters. Each simulation differs in the random placement (size, time and position) of the star formation events, as well as the in the x, y velocities of the stars at birth and their z -positions at the end of the simulation. As in all our simulations, each simulation provides the star counts at the final time (at $t = t_0 = 3$ Gyr) in 25 observational spheres centered at $z = 0$, $y = y_T/2$ and separated from each other by 1 kpc in the x direction. The front-side (inner edge) position of the strong arm at $y = y_T/2$ at the final moment of the simulation is $x_{f_s}(t_0, y_T/2) = 6.5$ kpc, whereas the front side position of the weak arm is located at $x_{f_w}(t_0, y_T/2) = 6.5 + x_T/2 = 19$ kpc. The arms move to the left in Figure 7 with respect to the stars orbiting the Galactic Center. Because our simulation area covers only 25 kpc (or about halfway) around the solar circle, only two of the four arms are within Figure 7.

The observational spheres located at the left of the front-side of the strong arm are those that have spent the most time without being crossed by a strong arm, and there-

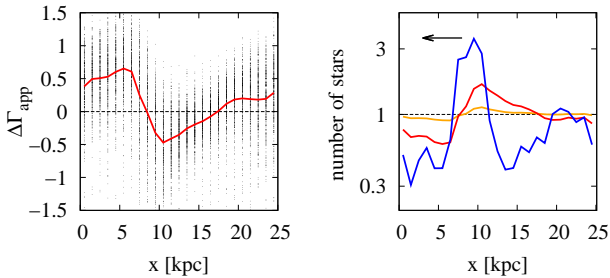


Figure 7. Effect of the spiral wave density for 2 strong and 2 weak arms (see text). Left panel: the dots represent all the $\Delta\Gamma_{\text{app}}$ values in 360 simulations, taking $r_{\text{obs}} = 200$ pc as the radius of our observing sphere. In each simulation 25 spheres are placed in the simulation area at intervals of $\Delta x = 1$ kpc along our 25 kpc simulation length. The red line connects the mean of the values of $\Delta\Gamma_{\text{app}}$ in the 360 simulations at each x point. The right panel shows the average number of stars that are within a sphere at position x in the 360 simulations normalized to the average number of stars per sphere. The blue, red and orange curves correspond respectively to stars of masses $m > 10$, $3 \leq m < 6$, and $1.5 \leq m < 3$. The arrow on the strong arm denotes the direction of the spiral arm with respect to the stars. The fraction of GMC formation in the interarm is $F_I = 0.3$; see text for other arm parameters.

fore are the ones where the population of the 3 to 6 M_{\odot} stars is most depleted. This is evidenced in the right panel of Figure 7, where the normalized abundance of stars in three stellar mass ranges ($m > 10$, $3 < m < 6$ and $1.5 < m < 3$) is shown. The stars with masses $m > 10$ display a normalized abundance (the blue curve) that closely follows the arms since their lifetimes are shorter than $\Delta x/v_a$. This creates the “beads on a string” appearance of external spiral galaxies. The stars in the mass range $3 < m < 6$ have lifetimes between 357 Myr and 64 Myr, whereas the time between successive passages of the spiral arms is ~ 260 Myr, so one expects a depletion of these stars between the arms. As shown in Figure 7 the amplitude of the spatial fluctuation of the abundance of these stars (the red curve) is considerably smaller than for the massive $m > 10$ stars but larger than the less massive stars in the range $1.5 < m < 3$, whose lifetimes span from 2570 Myr to 354 Myr. The amplitude of the spatial fluctuation decreases as the mass of the considered stars decreases because the corresponding increase in average age implies that lower mass stars (i) sample further back in time and therefore include stars formed in previous arm passages; and (ii) spread out farther from their birth sites due to their random velocities. As expected, to the left of the strong arm the population of the 3 to 6 M_{\odot} stars is more depleted than the population of the 1.5 to 3 M_{\odot} stars, and consequently in this region Γ_{app} is steeper than the underlying Γ . Note also that GMCs form stars during a period of $\tau_{\text{GMC}} \approx 20$ Myr and therefore the star formation is still enhanced along a distance $v_a \times \tau_{\text{GMC}} \sim 1$ kpc behind the back-side of the arm.

The left panel of Figure 7 shows the 360 values of $\Delta\Gamma_{\text{app}}$ in each sphere as well as the their local average (the red

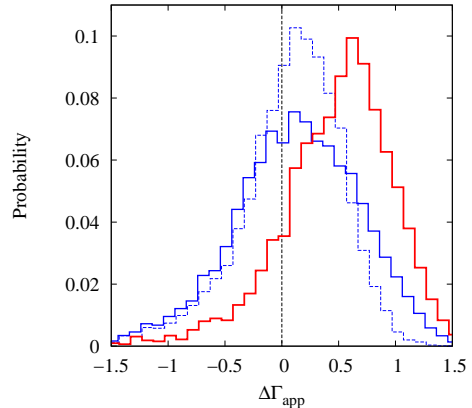


Figure 8. Distribution of $\Delta\Gamma_{\text{app}}$ when the effect of spiral arms in concentrating the GMCs is considered. In this model there are four arms, and 50% of the SFR occurs in the two strong arms, 20% occurs in the two weak arms, and 30% occurs in the interarm regions. The blue histogram includes all 9000 values of $\Delta\Gamma_{\text{app}}$ for all (arm and interarm) locations. The red histogram includes only the $\Delta\Gamma_{\text{app}}$ values in the observational spheres located in the interarm range $-2 < x < 7$ kpc in Figure 7 (see text). The dashed blue histogram corresponds to the standard case without the effect of spiral arms, as shown in Figures 2-5. Simulation parameters are $r_{\text{obs}} = 200$ pc, standard velocity distribution, and arm parameters given in text.

curve). It is clear that the imposed variation of the SFR has an important effect on the local average of $\Delta\Gamma_{\text{app}}$, but it is also clear that the dispersion of the $\Delta\Gamma_{\text{app}}$ values around the local average (due to the clustered star formation) is even larger than the departure of the local average from zero (that is, the departure of Γ_{app} from the underlying slope Γ).

The blue curve in Figure 8 displays the overall (arm and interarm) probability distribution of $\Delta\Gamma_{\text{app}}$ values for our standard 4-arm model with an observing radius of $r_{\text{obs}} = 200$ pc and our standard stellar velocity distribution. Comparison of the overall $\Delta\Gamma_{\text{app}}$ distribution with the case without the GMC concentration in the spiral arms (dashed blue curve) indicates that the spiral wave has a significant effect on the probability distribution, especially enhancing the probability in the high tail due to the depletion of high mass stars in the interarm regions. The standard deviation increases from 0.45 to 0.55 when GMC concentration in the spiral arms is considered. The red histogram represents the distribution of the $\Delta\Gamma_{\text{app}}$ values only in the nine spheres in the region that precedes the strong arm. Note that due to the periodic nature of our four arms model the spheres located in the range $-2 < x < 7$ kpc correspond to the spheres located in the ranges $23 < x < 25$ kpc and $0 < x < 7$ kpc in figure 7. At the final time of the simulation these spheres have left the the weak arm from 0 to 180 Myr ago and are being approached by the strong arm. As shown in Figure 7, in these spheres the average value of $\Delta\Gamma_{\text{app}}$ is above the average for the entire solar circle. In fact, in this interarm region the peak in the distribution occurs at $\Delta\Gamma_{\text{app}} \sim 0.65$, corresponding to $\Gamma_{\text{app}} = 2.0$ when the underlying $\Gamma = 1.35$.

Since the Gaia mission has the ability to sample volumes in the interarm region at the solar circle, Figure 9 shows the dependence of the spiral arm model to the volume sampled,

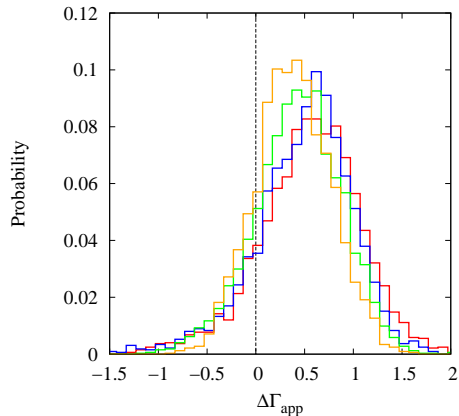


Figure 9. The same as Figure 8 but for different sizes of the observational volume. The red, blue, green and orange curves correspond to $r_{\text{obs}} = 100, 200, 400$ and 750 pc, respectively. For clarity only the histograms for $\Delta\Gamma_{\text{app}}$ in the interarm region are shown.

if the volume is kept in the interarm region. Because of the large distances between the arms, the effect of the spiral arm does not depend strongly on r_{obs} provided that r_{obs} is small compared to the distance to the corotation radius (we have assumed that v_a is constant in these simulations. The mean and median values of $\Delta\Gamma_{\text{app}}$ for a given volume are the same to within 2% so we just give mean values here. For $r_{\text{obs}} = 100, 200, 400,$ and 750 pc we find: mean $\Delta\Gamma_{\text{app}} = +0.52, +0.47, +0.41$ and $+0.36$; standard deviations are $0.55, 0.49, 0.44,$ and 0.38 ; probabilities that $\Delta\Gamma_{\text{app}} > 0.35$ are $0.67, 0.64, 0.57$ and 0.51 ; probabilities that $\Delta\Gamma_{\text{app}} > 0.65$ are $0.42, 0.38, 0.30, 0.23$. In short, for observing radii $r_{\text{obs}} = 100$ to 400 pc, there is a 67% to 57% chance to obtain $\Gamma_{\text{app}} > 1.7$ if the underlying $\Gamma = 1.35$ for our standard model of spiral arms at the solar circle. We look at results for other models below.

The purpose of this paper is to examine the observer/modeler determination of $\Gamma_{f,\text{app}} > 1.7$ in studies of local field PDMFs and how these values might be larger than the underlying Γ . Therefore, we present in Figure 10 the results of our simulations in a different way. We plot the probability of determining $\Gamma_{\text{app}} > 1.7$ as a function of the underlying Γ for five samples of local PDMFs on the solar circle. (1) The average of all positions along the solar circle, including all arm and interarm positions. (2) Regions in the strong arm (spheres located in the range $7 < x < 11$ kpc in Figure 7). Here, the enhanced population of GMCs and of star formation leads to lower probabilities that Γ_{app} will be higher than the underlying Γ , since these regions are well populated with massive stars. (3) The interarm region (spheres located in the range $-2 < x < 7$ kpc in Figure 7) that precedes the strong arm. Here, although low-mass stars have had time to migrate from arm locations, high-mass stars have had less time due to their shorter lifetimes and so they are underrepresented, leading to higher Γ_{app} values in these interarm regions. (4) The sphere centered at $x = 5.5$ kpc where the average value of Γ_{app} reaches its maximum. This curve provides an upper limit for this particular model of spiral arms at the solar circle. At the final time of the simulation this sphere has left the weak arm about 180 Myr ago and is being approached by the strong arm. (5) The

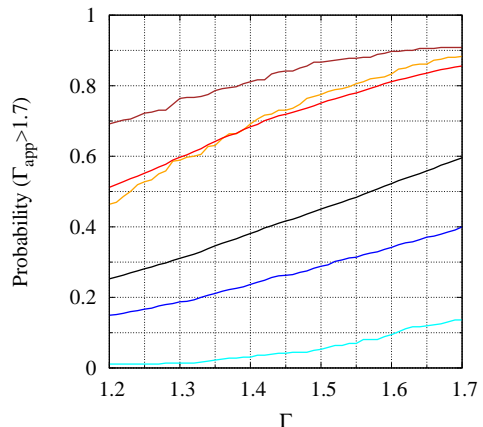


Figure 10. The probability that Γ_{app} will exceed 1.7 is plotted against the underlying Γ when the effect of spiral arms in concentrating the GMCs is considered. Simulation parameters are $r_{\text{obs}} = 200$ pc, standard velocity distribution, and arm parameters given in text. The black curve includes all (arm and interarm) 9000 values of Γ_{app} for all locations. The blue curve includes the Γ_{app} values in the strong arm region (spheres located in the range $7 < x < 11$ kpc of Figure 7). The red curve includes the Γ_{app} values in the interarm region that precedes the strong arm (spheres located in the range $-2 < x < 7$ kpc). The brown curve includes only the Γ_{app} values in the sphere centered at $x = 6.5$ kpc where the average value of Γ_{app} reaches its maximum. The cyan curve includes only the Γ_{app} values in the sphere centered at $x = 10.5$ kpc where the average value of Γ_{app} reaches its minimum. The orange curve includes only the Γ_{app} values in the sphere centered at $x = 1.5$ kpc where the Sun is assumed to be located at the final time of the simulation.

sphere centered at $x = 10.5$ kpc where the average value of Γ_{app} reaches its minimum. At the final time of the simulation this sphere is just leaving the strong arm. This curve provides a lower limit for this particular model of spiral arms at the solar circle. Finally, (6) The Sun is in an interarm region between the Sagittarius-Carina and the Perseus arms (e.g., Vallée (2005)), and we assume that the Sun is located at half way between the weak and the strong arms in the sphere centered at $x = 1.5$ kpc. Comparing the orange curve (for the assumed position of the Sun, which is close to the brown curve for the average over the interarm region) to the black (average over solar circle) curve, we conclude that the interarm location of the Sun can significantly (by a factor $\sim 1.5 - 2$) raise the likelihood that a local measurement of Γ_{app} will exceed 1.7 when the underlying universal slope Γ is less than this value. The median value of $\Delta\Gamma_{\text{app}}$ for the $-2 < x < 7$ kpc interarm region is 0.51. As result, for example, if the underlying $\Gamma = 1.35$, there is approximately 50% chance that a local measurement with observing radius 200 pc will obtain $\Gamma_{f,\text{app}} > 1.86$.

Finally, we make a rough estimate the uncertainty in our spiral arm model by presenting the results from simulations that use other parameters. We have run our standard spiral arm model but with the Miville-Deschênes et al. (2017) distribution of GMCs by mass. Although these two GMC distributions gave very different results for the probability that $\Delta\Gamma_{\text{app}} > 0.35$ when the GMCs were formed at random positions at the solar circle (0.15 for Miville-Deschênes et al. (2017) versus 0.27 for WM97), when the effect of spiral arms

is included, they differ very little (0.62 versus 0.64) in the interarm region (3). The reason is that the main effect is that the SFR has been suppressed compared to its average solar circle value for roughly 90 Myr, and how the molecular mass is distributed does not matter significantly.⁴ We have also run a case where the fraction of GMC formation in the interarm is $F_I = 0.5$ and where $F_S = 0.33$. These parameters imply that the relation of the star formation rate per unit area in the strong-arm, weak-arm and interarm regions is respectively 3:1.5:1. For $r_{\text{obs}} = 200$ pc and considering only the interarm region described as (3) above, we find that for this case the probability of $\Delta\Gamma_{\text{app}} > 0.35$ is 0.47, as opposed to 0.64 for our standard model.

5 SUMMARY AND CONCLUSIONS

Many observations of young clusters in the Galaxy, as well as global observations of external galaxies, suggest that the underlying high-mass IMF slope is of order the Salpeter value, $\Gamma = 1.35$, or equivalently that $1.2 \lesssim \Gamma_c \lesssim 1.7$. However, recent observations of stars within $r_{\text{obs}} \simeq 100$ pc of the Sun (Dawson & Schröder 2010), $r_{\text{obs}} \simeq 200$ pc (Rybizki & Just 2015), and $r_{\text{obs}} \sim 300$ pc (Czekaj et al. 2014) have led to apparent high-mass slopes $\Gamma_{f,\text{app}} \simeq 1.7 - 2.1$. The goal of this paper is to reconcile these apparently contradictory observations in the context of an overall universal IMF.

We have modeled the inhomogeneous distribution of stars at the solar circle caused by the facts that (1) they are born in localized GMCs and then randomly move to fill the inter-GMC regions and (2) that the Sun is in an interarm region of the Galaxy. Higher mass stars do not live as long as solar mass stars. They therefore retain a memory of their birth sites and their surface density distribution is more inhomogeneous. In our model, we treat the age-dependent vertical scale heights of stars and consider two star formation histories: the standard history is that the average star formation rate has declined as $\exp(-t/8.3\text{Gyr})$, but we also consider a constant average star formation rate over the last 3 Gyr. However, we show that within our simulations our results are very nearly independent of the models utilized for the SFH or the vertical diffusion. We defined $\Gamma_{\text{app},12}$ as the apparent value of the high-mass slope after allowing for stellar evolution, the star formation history, and age-dependent vertical diffusion. For star formation that is spatially and temporally constant in the plane, this apparent value of the slope is equal to the underlying actual slope. Observers generally allow for these effects, so insofar as their models for the SFH and vertical diffusion are correct, they would find the correct value of Γ in this uniform case. However, clustering of star formation due to the fact that many stars are born in massive GMCs that are well separated and to the effects of spiral arms causes the apparent Γ_{app} to differ from Γ (for simplicity, we dropped the subscript 12 in Section 2.4). We then defined $\Delta\Gamma_{\text{app}} \equiv \Gamma_{\text{app}} - \Gamma$ and showed that the distribution of $\Delta\Gamma_{\text{app}}$ that result from sampling various small volumes at the solar circle is independent of the underlying Γ if $1.2 < \Gamma < 1.7$.

Our numerical models treat an area of 37.5 kpc^2 : 25 kpc around the solar circle and 1.5 kpc in radial extent. In that area, we form GMCs with their observed mass distribution and at a rate such that the current surface density of GMCs matches observation. We assume that a GMC lasts for 20 Myr. Inside each GMC, stars form during the duration of the GMC and convert 3.8% of the mass of the cloud to stars. We form stars with mass $m = 1.5 - 6$ (solar masses) assuming a power law IMF in this “high-mass” region that goes as $m^{-\Gamma}$. We give each star a random velocity chosen from a velocity dispersion relation observed for these stars in the plane of the Galaxy at the solar circle and follow their motion in the Galactic plane. The simulation follows the time evolution of roughly 2×10^7 stars with $m = 1.5 - 6$ for 3 Gyr. The 3 Gyr ensures that we fully sample the PDMF of all the stars in this mass range, since the lowest mass (i.e., longest lived) star in the simulation ($m = 1.5$) has a main sequence lifetime of 2.6 Gyr.

In each global simulation we stop the evolution after 3 Gyr, and then construct 25 independent small (radius $r_{\text{obs}} = 100 - 750$ pc) spheres inside the global simulation, and measure the ratio $\mathcal{R} \equiv \mathcal{N}_*(1.5 < m < 3) / \mathcal{N}_*(3 < m < 6)$. The ratio is a measure of the PDMF of the stars in this mass range and inside the given small volume. We then run ~ 360 global simulations, so that we have a large number (9000) of small volumes for statistical analysis. We compare the \mathcal{R} value obtained in each volume with the ratio that would be obtained for a given underlying Γ and with corrections for the SFH and the vertical segregation of stars of different age. As noted above, this comparison provides an apparent value for the high-mass slope, Γ_{app} . This Γ_{app} can differ from the underlying global Γ because the stars in the small observed volume may have a deficit or an excess of higher mass stars compared to lower mass stars (i.e., the PDMFs in small volumes can vary from the PDMF taken over the whole solar circle). As expected, our models show that the distribution narrows around the underlying Γ (i.e., $\Delta\Gamma_{\text{app}}$ goes to zero) as the random velocity dispersion of the stars increases, as the stellar formation sites are more uniformly distributed, and as the observational volume increases, since all these effects tend to homogenize the stellar populations. We present distribution functions of $\Delta\Gamma_{\text{app}}$, which show, for example, that for randomly placed observing volumes with radii of 600-100 pc, there is a roughly 17-33% chance that local observations of the solar neighborhood would result in the inference of $\Delta\Gamma_{\text{app}} \gtrsim 0.35$. For our standard case $r_{\text{obs}} = 200$ pc we show that the range of GMC mass distributions in the current literature leads to variations in this chance from 15% to 27%. In other words, there is a moderate probability that the observed Γ_{app} could be $\gtrsim 1.7$ when the underlying universal $\Gamma = 1.35$.

The value of Γ_{app} inferred from observations can also be affected by spiral arms, as noted by Elmegreen & Scalo (2006). There is strong evidence that the Sun currently lies in an interarm region that is somewhat devoid of recent star formation. Using observations that suggest that the SFR in the interarm region is $\sim 30\%$ of the total SFR in external spiral galaxies, we present curves (Figure 9) that show the probability of $\Gamma_{\text{app}} \gtrsim 1.7$ as a function of the underlying Γ for various samples in arm and interarm regions. We conclude that the probability of inferring $\Gamma_{\text{app}} \gtrsim 1.7$ in the solar neighborhood is ~ 0.6 for $\Gamma = 1.35$ and for observing radii

⁴ For similar reasons, as discussed above, there is not much dependence on the observing volume.

$r_{\text{obs}} \lesssim 500$ pc. If the SFR in the interarm region is $\sim 50\%$ of the total SFR, this probability is reduced to ~ 0.5 . We therefore propose that the apparent conflict of more global estimates of $\Gamma \sim 1.35$, or $1.2 \lesssim \Gamma \lesssim 1.7$, with more local observations of $\Gamma_{f,\text{app}} \simeq 1.7 - 2.1$ is caused by the inhomogeneities in the spatial distribution of stars, which increases with stellar mass, and by the fact that the Sun lies currently in an interarm region of diminished GMC and star formation.

We are further motivated by the data that is becoming available from ESA's Gaia mission, which will enable a determination of both the average PDMF in the Galaxy and its spatial fluctuations. As we have shown, spatio-temporal variations in the SFR, due to formation of stars in both clusters and in spiral arms, lead to spatial variations of the PDMF that can be directly measured by Gaia. This will provide powerful constraints on relative SFR in the arm and interarm regions; as noted in Appendix B, this should become clearer near the corotation radius. It will be more challenging to separate variations in the PDMF due to clustering from those due to variations in the IMF, but this should be possible using information on stellar velocities, at least for the younger stars. Our work is but a first step, showing how clustering affects local PDMFs.

ACKNOWLEDGEMENTS

We acknowledge valuable input from M. Aumer, J. Bland-Hawthorn, C. Dobbs, R. Genzel, K. Masters, M. Miville-Deschenes, E. Ostriker, S. Ragan, and D. Soderblom. We also thank the referee for a careful reading of the original manuscript and for numerous suggestions that improved the clarity and organization of the paper. The research of CFM is supported in part by NASA ATP grant NNX13AB84G.

REFERENCES

Arenou, F. 2011, American Institute of Physics Conference Series, 1346, 107
 Ashworth, G., Fumagalli, M., Krumholz, M. R., et al. 2017, MNRAS, 469, 2464
 Aumer, M., & Binney, J. J. 2009, MNRAS, 397, 1286
 Aumer, M., Binney, J., & Schönrich, R. 2016, MNRAS, 462, 1697
 Azimlu, M., Marciniak, R., & Barmby, P. 2011, AJ, 142, 139
 Bastian, N., Covey, K. R., & Meyer, M. R. 2010, ARA&A, 48, 339
 Benjamin, R. A. 2008, Massive Star Formation: Observations Confront Theory, 387, 375
 Blaauw, A. 1991, NATO Advanced Science Institutes (ASI) Series C, 342, 125
 Bressan, A., Marigo, P., Girardi, L., et al. 2012, MNRAS, 427, 127
 Cappellari, M., McDermid, R. M., Alatalo, K., et al. 2012, Nature, 484, 485
 Chabrier, G. 2005, The Initial Mass Function 50 Years Later, 327, 41
 Chomiuk, L., & Povich, M. S. 2011, AJ, 142, 197 (CP11)
 Churchwell, E., Babler, B. L., Meade, M. R., et al. 2009, PASP, 121, 213
 Czekaj, M. A., Robin, A. C., Figueras, F., Luri, X., & Haywood, M. 2014, A&A, 564, A102
 Dawson, S. A., & Schröder, K.-P. 2010, MNRAS, 404, 917
 Dehnen, W., & Binney, J. 1998, MNRAS, 294, 429
 Drimmel, R., & Spergel, D. N. 2001, ApJ, 556, 181

Drimmel, R., Cabrera-Lavers, A., & López-Corredoira, M. 2003, A&A, 409, 205
 Elmegreen, B. G., & Scalo, J. 2006, ApJ, 636, 149
 Foyle, K., Rix, H.-W., Walter, F., & Leroy, A. K. 2010, ApJ, 725, 534
 Georgelin, Y. M., & Georgelin, Y. P. 1976, A&A, 49, 57
 Hennebelle, P., & Falgarone, E. 2012, A&ARv, 20, 55
 Heyer, M., & Dame, T. M. 2015, ARA&A, 53, 583
 Hopkins, P. F. 2012, MNRAS, 423, 2037
 Just, A., & Jahreiß, H. 2010, MNRAS, 402, 461
 Koo, B.-C., Park, G., Kim, W.-T., et al. 2017, PASP, 129, 094102
 Kroupa, P., Weidner, C., Pflamm-Altenburg, J., et al. 2013, Planets, Stars and Stellar Systems. Volume 5: Galactic Structure and Stellar Populations, 5, 115
 Kroupa, P., & Weidner, C. 2003, ApJ, 598, 1076
 Lee, E. J., Murray, N., & Rahman, M. 2012, ApJ, 752, 146
 Lee, J. H., Hwang, N., & Lee, M. G. 2011, ApJ, 735, 75
 Li, Z., Gerhard, O., Shen, J., Portail, M., & Wegg, C. 2016, ApJ, 824, 13
 Lu, J. R., Do, T., Ghez, A. M., et al. 2013, ApJ, 764, 155
 McKee, C. F., Parravano, A., & Hollenbach, D. J. 2015, ApJ, 814, 13
 McKee, C. F., & Williams, J. P. 1997, ApJ, 476, 144
 Miville-Deschênes, M.-A., Murray, N., & Lee, E. J. 2017, ApJ, 834, 57
 Muzic, K., Schoedel, R., Scholz, A., et al. 2017, arXiv:1707.00277
 Nordström, B., Mayor, M., Andersen, J., et al. 2004, A&A, 418, 989
 Offner, S. S. R., Clark, P. C., Hennebelle, P., et al. 2014, Protostars and Planets VI, 53
 Paresce, F., & De Marchi, G. 2000, ApJ, 534, 870
 Parravano, A., McKee, C. F., & Hollenbach, D. J. 2006, Revista Mexicana de Física Supplement, 52, 1
 Parravano, A., McKee, C. F., & Hollenbach, D. J. 2011, ApJ, 726, 27 (Paper I)
 Prantzos, N. 2008, EAS Publications Series, 32, 311
 Reid, M. J., Menten, K. M., Brunthaler, A., et al. 2014, ApJ, 783, 130
 Renzini, A. 2005, The Initial Mass Function 50 Years Later, 327, 221
 Rice, T. S., Goodman, A. A., Bergin, E. A., Beaumont, C., & Dame, T. M. 2016, ApJ, 822, 52
 Robitaille, T. P., Churchwell, E., Benjamin, R. A., et al. 2012, A&A, 545, A39
 Rosolowsky, E. 2005, PASP, 117, 1403
 Rybizki, J., & Just, A. 2015, MNRAS, 447, 3880
 Scalo, J. M. 1986, Fundamentals Cosmic Phys., 11, 1
 Scalo, J. 2005, The Initial Mass Function 50 Years Later, 327, 23
 Schneider, F. R. N., Sana, H., Evans, C. J., et al. 2018, Science, 359, 69
 Schröder, K.-P., & Pagel, B. E. J. 2003, MNRAS, 343, 1231
 Solomon, P. M., Rivolo, A. R., Barrett, J., & Yahil, A. 1987, ApJ, 319, 730
 Vallée, J. P. 2005, AJ, 130, 569
 Vallée, J. P. 2014, AJ, 148, 5
 Vallée, J. P. 2017, Ap&SS, 362, 79
 van Dokkum, P. G., & Conroy, C. 2010, Nature, 468, 940
 Weisz, D. R., Johnson, L. C., Foreman-Mackey, D., et al. 2015, ApJ, 806, 198
 Williams, J. P., & McKee, C. F. 1997, ApJ, 476, 166

APPENDIX A. STELLAR VELOCITY DISPERSION

The stellar velocity dispersion $\sigma(\tau)$ increases with the age τ of the star due to gravitational encounters with GMCs. We consider three possible evolutions of the stellar velocity dispersion with age τ of the star: an upper limit, a lower limit, and an intermediate standard expression. For our upper limit of the velocity dispersion, we adopt the functional form given by [Aumer et al. \(2016\)](#),

$$\sigma_{\text{ABS}}(\tau) = \sigma_1 \left(\frac{\tau + \tau_1}{1 + \tau_1} \right)^\mu, \quad (1)$$

where the age τ is expressed in Gyr. In Table 3 we give parameter values of Equation (1) in the radial and azimuthal directions that fit the observational estimates at the solar circle derived by [Nordström et al. \(2004\)](#) and by [Dehnen & Binney \(1998\)](#) for $0.5 < \tau < 3$ Gyr. We adopt this expression for all ages of the stars in the simulation (i.e., $0 < \tau < 2.57$ Gyr, the lifetime of a $m = 1.5$ star). It is an upper limit because this expression overestimates the dispersion for $\tau < 0.5$ Gyr as explained below.

Table 3. $\sigma_{\text{ABS}}(\tau)$ parameters

	R	ϕ
σ_1 (km s ⁻¹)	22	13
τ_1 (Gyr)	0.3	0.4
μ	0.31	0.34

This fit to the velocity dispersion is not accurate for ages less than ~ 500 Myr (Aumer, private communication); in particular, it gives velocity dispersions at birth [$\sigma_{\text{ABS}}(0) = (14, 8.5)$ km s⁻¹ for the radial and azimuthal velocities, respectively] significantly greater than observed. [Aumer et al. \(2016\)](#) estimate that due to random motions of the stars at birth and also of the GMCs in which they form, the initial ($\tau = 0$) velocity dispersions in both the radial and azimuthal directions is of order 6 km s⁻¹. We are mostly interested in the velocities dispersions of the $m \sim 3$ stars, since it is their spatial inhomogeneity that drives the dispersion in Γ_{app} . Since they live typically for only ~ 300 Myr, their dispersions lie in the range where σ_{ABS} would provide an overestimate. For our standard expression for the velocity dispersion, we assume that during the first 500 Myr σ increases linearly from its initial value to the ABS value as

$$\sigma(\tau) = \left[1 - \left(\frac{\tau}{0.5 \text{ Gyr}} \right) \right] 6 \text{ km s}^{-1} + \left(\frac{\tau}{0.5 \text{ Gyr}} \right) \sigma_{\text{ABS}}(\tau). \quad (2)$$

After the first 500 Myr we assume that the velocities equal $\sigma_{\text{ABS}}(\tau)$; in particular, at $\tau = 0.5$ Gyr, we have $\sigma_{\text{ABS}} = (19, 11)$ km s⁻¹, respectively. Finally, for the third possible evolution, we adopt the lower limit of 6 km s⁻¹ in each direction for all τ .

To set the mean speed in the plane of a particular star, we pick the speeds s_x and s_y from a Gaussian distribution with standard deviations $\langle \sigma_\phi \rangle(\tau)$ and $\langle \sigma_R \rangle(\tau)$, respectively, where $\langle \sigma \rangle(\tau)$ is the mean velocity dispersion from when the star was born to the end of the simulation, when the star has an age τ . With that velocity, we then move the star from its birth location to its final x, y location at the end of the simulation. We assume periodic boundary conditions, so

that, for example, a star that crosses the radial (y) boundary is introduced at the other radial boundary at the same x with the same velocity. Similarly, a star that crosses the azimuthal (x) boundary is introduced at the other azimuthal boundary at the same y with the same velocity.

The vertical component of velocity sets the scale height of a star of a certain age τ . Equation (22) in the text describes how we account for the time-evolving scale height of the stars.

APPENDIX B. SPIRAL ARM MODEL

To consider the effect of the spiral arms we assume that the probability of formation of GMCs is enhanced in the arm regions. This is the only effect of spiral arms in our model: the positions where GMCs form are modified, but not their mass or the global formation rate of GMCs. We consider that the spiral arm is a global density wave. We assume a four-arm model with two strong and two weak arms (see Section 4), where a fraction F_S and F_W of the GMCs formed in strong and weak arms, respectively. The fraction of GMCs formed in the interarm is then $F_I = 1 - F_S - F_W$. The value of $F_S + F_W$, the fraction of stars born in GMCs that were formed in the arms, is uncertain at the solar circle. We therefore use observations of the spiral galaxies NGC5194, NGC 628, NGC 6946, M51, and M31 made by [Foyle et al. \(2010\)](#), [Azimlu et al. \(2011\)](#), and [Lee et al. \(2011\)](#) to estimate $F_S + F_W = 0.7$. This implies that $F_I = 0.3$ or that roughly 30% of the star formation is in interarm regions (these references find a range of values $F_I \sim 0.1$ to 0.6, so our standard model should be considered exemplary. We also treat the case where $F_I = 0.5$, $F_S = 0.33$ and $F_W = 0.17$. In our standard case we adopt $F_I = 0.3$, $F_S = 0.5$ and $F_W = 0.2$. Gaia should help determine these numbers.

Besides F_S , F_W , and the number of arms, the properties of the spiral arm model are fixed by the pitch angle, $\alpha = 12^\circ$ ([Vallée \(2005\)](#)), the full arm width measured normal to the arm, Δ_a , and the arm velocity with respect to the LSR, v_a . We adopt $\Delta_a = 0.8$ kpc from the results summarized by [Vallée \(2014\)](#). We do not vary the phase of the spiral structure in our modeling and simply place the Sun in a typical interarm position. Note that the width of the intersection of the arm and the solar circle is $\Delta_x = \Delta_a / \sin \alpha = 3.8$ kpc, a few times larger than Δ_a . Moreover, a GMC that forms within an arm continues to form stars for about 20 Myr, and as a result the x -width of enhanced star formation region is more than a kpc wider than the enhanced GMC formation region. Finally, $v_a = R_0 \Omega_p - v_c$, where the angular velocity of the spiral pattern, Ω_p , is estimated to lie in the range (20 - 25) km s⁻¹ kpc⁻¹ ([Li et al. 2016](#); [Vallée 2017](#)). Taking the average value of Ω_p and adopting $R_0 = 8.3$ kpc (rounded from 8.34 ± 0.16 kpc - [Reid et al. 2014](#)) and a circular velocity $v_c = 240$ km s⁻¹ [Reid et al. \(2014\)](#), we find $v_a \simeq -50$ km s⁻¹. This implies that it takes 260 Myr to travel from the front of one arm to the front of the next; the time spent in the interarm region, neglecting velocity changes in the arms, is about 180 Myr. For these parameter values, the azimuthal (x) position of an arm at the top and bottom of the simulation area ($y_T = 1.5$ kpc) differs by $y_T / \tan \alpha = 7.05$ kpc. Since the length of simulation area in the x direction ($x_T = 25$ kpc) is

about half of the solar circle length, the separation between arms is about $x_T/2$ in a 4-arm model.

In our simple model the star motions are not modified by their interaction with the spiral structure (except implicitly through the dependence of σ on τ). As seen from the north Galactic pole, the stars and spiral pattern rotate clockwise, but since the solar circle lies within the corotation radius, $R_{\text{CR}} = v_c/\Omega_p \simeq 10.5$ kpc. the arm velocity with respect to the LSR is negative in our x, y coordinates.

All the results presented in this paper are for the solar circle. If the observation volumes are placed at different Galactocentric radii R , the time spent in the interarm region first increases with R up to the corotation radius and then decreases. As consequence, the probability of finding large values of $\Delta\Gamma_{\text{app}}$ will reach a maximum at the corotation radius. Beyond that radius, the dispersion of $\Delta\Gamma_{\text{app}}$ would decrease with R , as long as the properties of the spiral arms and the stellar diffusion remain about the same.

For a simulation area where $x_T = 25$ kpc and $y_T = 1.5$ kpc, or $x_T \gg y_T$, the front-side and the back-side of an arm (in our model of the Milky Way, this corresponds to the inner and outer sides), can be described as

$$x_f(y, t) = x_0 - \frac{y}{\tan \alpha} - v_a(t_0 - t) \quad (3)$$

and

$$x_b(y, t) = x_f(y, t) + \frac{\Delta_a}{\sin \alpha}, \quad (4)$$

where $x_0 = x_f(y=0, t=t_0)$ is the final front-side arm position at $t = t_0$ and $y = 0$. In the frame of the simulation area and as seen from the north Galactic pole the arms move to the left since the Sun is inside corotation ($v_a < 0$) and the arm is tilted to the left when $0 < \alpha < \pi/2$. Outside corotation, v_a is positive.

The first step in determining the location of a GMC formed at time t is to set its y position at random in the range 0 to y_T . After that choice, the position of the front and back side of the arm are determined using Equations (3,4), and finally the x position is picked from the probability distribution $dP(t, y, x)/dx$ in the x range from 0 to x_T :

$$\frac{dP(t, x, y)}{dx} = \quad (5)$$

$$\begin{cases} F_S/\Delta_x & \text{if } (x, y) \text{ is within a strong arm at time } t, \\ F_W/\Delta_x & \text{if } (x, y) \text{ is within a weak arm at time } t, \\ F_I/(x_T - 2\Delta_x) & \text{if } (x, y) \text{ is in the interarm region at time } t, \end{cases} \quad (6)$$

where $\Delta_x = \Delta_a/\sin \alpha$.

This paper has been typeset from a $\text{\TeX}/\text{\LaTeX}$ file prepared by the author.